Accelerated inversion recovery MRI of the myocardium using spiral acquisition

Beschleunigte Inversion-Recovery MR-Bildgebung des Myokards mit spiralen Auslesezügen

Doctoral thesis for a doctoral degree
at the Graduate School of Life Sciences,
Julius-Maximilians-Universität Würzburg,
Section Biomedicine
submitted by

Johannes Portmann
born in Lübbecke

Würzburg, 2022

Submitted on the 29.09.2022

Members of the Thesis Committee:

Primary Supervisor:	Prof. Dr. Herbert Köstler
Second Supervisor:	Prof. Dr. Michael Laßmann
Third Supervisor:	PD Dr. Dr. Bernhard Petritsch
Chairperson:	Prof. Dr. Peter Jakob

Date of Public Defense: 07.02.2023

Date of Receipt of Certificates: .....

This is how we know that we belong to the truth and how we set our hearts at rest in his presence: If our hearts condemn us, we know that God is greater than our hearts, and he knows everything.

(1. John 3:19–20, Bible, New International Version)

Contents

1 Introduction

Large parts of the findings regarding the method of IR-CRISPI presented in this work were previously published in *NMR in Biomedicine* by John Wiley & Sons, Inc.[39] under the Creative Commons Attribution-NonCommercial License (CC BY-NC 4.0)*. Figures that were replicated in this work (entirely or in parts) are declared accordingly.

1.1 Motivation

Magnetic Resonance Imaging (MRI) is the gold standard modality for a broad spectrum of medical soft tissue exams. Firstly, this is the case because the measuring process does not harm the patient. The most common substitute of MRI, computed tomography (CT), however, means patient exposure to X-ray radiation. MRI, secondly, yields very high contrast between different types of soft tissue, with a broad variety of adjustment options.

One of the greatest drawbacks of MRI, though, is the long acquisition time. This, unfortunately, becomes especially obstructive while trying to image a moving organ such as the heart. Consequently, cardiovascular MR (CMR) measurement times of one hour are common.[40] Simultaneously, they are prone to contain motion artifacts and other imaging errors. Two of the most frequently applied CMR protocols are the cine[9] measurement for the assessment of myocardial morphology, kinetics and cardiac function, and late gadolinium/delayed gadolinium enhancement (LGE) imaging[50] for the assessment of myocardial viability. Latter exam is contrast enhanced, enabling the imaging of chronic and acute myocardial infarction, of fibrotic and inflamed tissue.[17,20] Conventionally, the corresponding measurement protocols are being acquired in a segmented pattern over several heartbeats in breath-hold.[28]

This doctoral thesis is an attempt to accelerate the CMR exam without loss of its advantageous properties. In CMR, this can be achieved by exploiting the fact that the patient is not moving for the greater part and

*https://creativecommons.org/licenses/by-nc/4.0/

the occurring respiratory and cardiac motion happens periodically. As a result of research in this field, real-time acquisition techniques[3,45] enable imaging without repetition and retrospective data reassembly. For that matter, particularly non-Cartesian sampling schemes and compressed sensing techniques[5,12,30,53] contribute to the improvement of spatial and temporal resolution.

As consequence of the acceleration, not only becomes time at the MR-scanners more available,[40] but because of shorter measurement times patients with cardiovascular diseases, who often experience problems to hold their breath, can receive a more adequate exam. As real-time acquisitions are clearly less susceptible to motion artifacts, sometimes even the quality of imaging can be improved.

On this account, I developed real-time acquisitions by implementing two ways to exploit temporal redundancy using spiral sampling, which is enhanced by a preceding trajectory correction.[46] In this doctoral thesis I will explain their concepts in detail. Their limitations as well as their advantages over the conventional CMR exam will be highlighted.

1.2 Outline

In the following, firstly, the fundamentals of MRI and after that basics related to the presented research are explained. Secondly, conventional cardiovascular applications are introduced (see section 2). In methods (3) and results (4), two newly developed techniques, MOCO-MAP and IR-CRISPI, which comprise the main part of this doctoral work, are described first with respect to concept and way of application, then with respect to the findings originating for the most part from volunteer and patient studies. In discussion (5) the findings are being evaluated, respectively, and in conclusion (6) a final statement for both techniques is given. Afterwards, summaries in English (7) and German (8) are provided.

1.3 MRI basics

MRI is a broadly used tool for imaging and assessing a multitude of body parts and characteristics, such as organ structure and quantifying its function. Although an exhaustive physical explanation of MRI goes beyond the scope of this work, accelerated cardiac imaging using the MR scanner and my research in this field shall be presented as intelligibly as possible and without leaving out important details. (A reference for deeper insight into MR basics is provided.[4])

1.3.1 MR signal

The first important question in explaining MRI is where the MR information comes from. The signal, which is being measured at the MR scanner, is the answer of the nuclear spin on a pulsed radio-frequency input.

The spin is defined as discrete intrinsic angular momentum. Thus, ${}^{1}_{1}$H-hydrogen is best-suited for imaging purposes. It has the highest spin to mass ratio of 1/2 to 1 u and the highest absolute number of atoms in the human body, which mainly consists of water and fat. Nevertheless, for special MR exams other nuclei can be used, e. g. sodium imaging for the exam of cell function.[32]

In the 1920's, Otto Stern and Walther Gerlach observed the quantized nature of the electron spin in a spatially varying magnetic field. Although the electrons were part of uncharged silver atoms, not only did the magnetic field divert the particle beam, but it was split and the particles were guided towards two different directions. Reason for this is the spin of the electrons.[4] As electrons by themselves are charged particles and silver contains one unpaired electron, the spin results in a discrete magnetic momentum. Just like the electron, the proton is a spin-$\frac{1}{2}$ particle, meaning its quantum number s is exactly $\frac{1}{2}$. The absolute value of its spin is given by

$$|\vec{I}| = \hbar\sqrt{s(s+1)} = \frac{\sqrt{3}}{2}\hbar \tag{1}$$

and one component of the spin I_z is determined using the magnetic quantum

number ($m_s \coloneqq -s, -s+1..., s$),

$$I_z = \hbar m_s = \pm\frac{1}{2}\hbar, \tag{2}$$

with $\hbar$ being the reduced Planck's constant.

A nuclear spin $\vec{I}$ then results in the magnetic dipole moment $\vec{\mu}$ given as

$$\vec{\mu} = \gamma_p \vec{I}. \tag{3}$$

γ_n is the gyromagnetic ratio, which is dependent on the type of particle. Because of the equivalence of spatial directions, states of different m are degenerate regarding their energy. The application of a magnetic field, however, yields discrete energy levels. With (3) the spin component I_z parallel to the magnetic field $\vec{B} = (0, 0, B_z)^T$ and the potential energy $E = -\vec{\mu} \cdot \vec{B}$ leave the two possible states

$$E = \pm\frac{\hbar}{2}\gamma_p B_z. \tag{4}$$

With the Boltzmann distribution one can calculate the ratio of particles in either state:

$$\frac{N_-}{N_+} = \exp\left(-\frac{\Delta E}{k_B T}\right) = \exp\left(-\frac{\gamma_p \hbar B_z}{k_B T}\right) \tag{5}$$

with N_+ spins facing the direction of the magnetic field vector and N_- spins facing the opposite direction. k_B is the Boltzmann constant and T the temperature. This quotient is very close to, but smaller than, 1, which means the fraction of the spins in parallel direction outweighs the spins in anti-parallel direction, resulting in a macroscopic magnetization. The resulting macroscopic magnetization for small changes (Curie's law) can be approximated as

$$\vec{M_0} \approx \frac{\rho_0 \gamma_p^2 \hbar^2}{4 k_B T} \vec{B_0}. \tag{6}$$

I_z always just amounts to $\frac{1}{\sqrt{3}}$ times $|\vec{I}|$ (eqs. 1 and 2), so there is a residual

spin component, which is perpendicular to the magnetic field and leads to a torsional moment.

$$\vec{D} = \vec{\mu} \times \vec{B} \tag{7}$$

$$\frac{\mathrm{d}\vec{\mu}}{\mathrm{d}t} = \gamma_p \vec{\mu} \times \vec{B_0} \tag{8}$$

This results in a constant precession of the spins with Larmor frequency ω_0, which equals $\gamma_p|\vec{B_0}|$. By application of a rotating magnetic field $\vec{B_1}(t)$ in form of a radio-frequency (RF) pulse, it is possible to add a second "precession" (ω_1), see the coordinate system in figure 1. That way the macroscopic magnetization turns by the flip angle

$$\alpha = \int_0^\tau \omega_1 \mathrm{d}t = \gamma_p \int_0^\tau |\vec{B_1}| \mathrm{d}t. \tag{9}$$

As the plane in which the excitation is induced is identical for all spins (still just a very small fraction of spins is being excited), they now precede in phase. A macroscopic signal can be measured with a receiving coil, best placed near to the excited object.

The transverse magnetization relaxes exponentially to the ground state mainly because of dipole-dipole interactions with the surrounding tissue. Here, two tissue specific parameters are being defined: T_1 characterizes the time until the magnetization returns to ground state ($\vec{M}||\vec{B_0}$) and T_2 characterizes the time it takes for the spins to dephase. In total, T_1, T_2, and the spin density ρ are responsible for the intensity distribution on the MR image.

1.3.2 K-space sampling

The next step in understanding MR imaging is knowing how to locate the described signal. By superposition of $\vec{B_0}$ with a spatially constant gradient field $\vec{G} = \nabla|\vec{B}|$ the Larmor frequency becomes dependent on the location $\vec{r}$

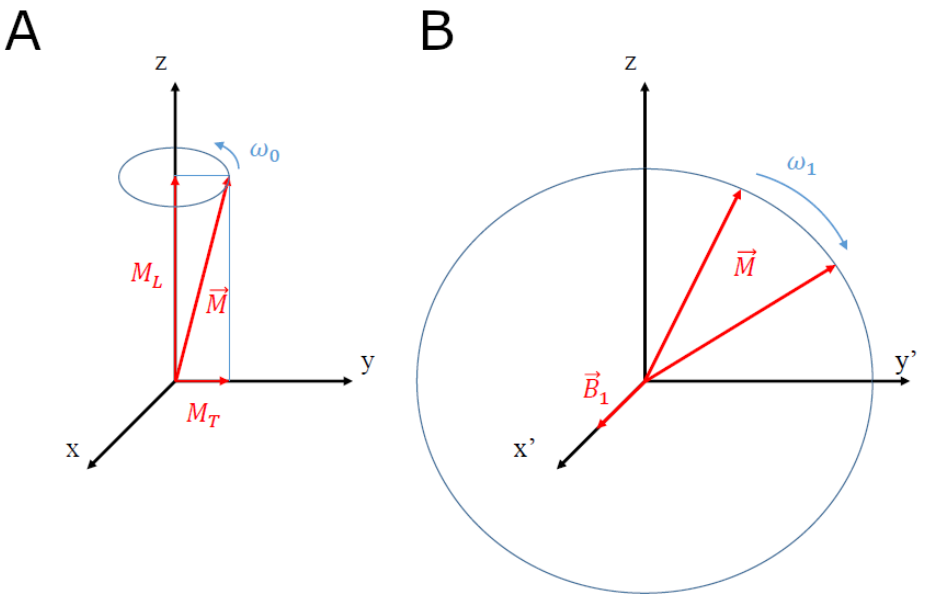

Figure 1: A: precession ω_0 of the magnetization around the z-axis (with $\vec{B_0}||\vec{e_z}$). B: For a coordinate system that rotates with ω_0 around the z-axis (x→x', y→y'), a secondary magnetic field ($\vec{B_1}||\vec{e_{x'}}$) results in a secondary precession in the plane perpendicular to the x'-axis.)

accordingly:

$$\omega(\vec{r},t) = \omega_0 + \gamma_p \vec{G}(t)\vec{r} \tag{10}$$

The spin density $\rho(\vec{r})$ to measure yields the signal

$$\begin{aligned} K(t) \sim & \int_{-\infty}^{\infty} \rho(\vec{r}) \exp\left(\mathrm{i}\int_0^T \omega(\vec{r},t)dt\right) \mathrm{d}^3\vec{r} \\ \sim \exp(i\omega_0 T) & \int_{-\infty}^{\infty} \rho(\vec{r}) \exp\left(\mathrm{i}\gamma_p \int_0^T \vec{G}(t)dt\vec{r}\right) \mathrm{d}^3\vec{r}. \end{aligned}$$

With the substitution of $\vec{k} = \gamma_p \int_0^T \vec{G}(t)dt$ the familiar Fourier relationship appears:

$$K(\vec{k}) \sim \int_{-\infty}^{\infty} \rho(\vec{r}) e^{\mathrm{i}\vec{k}\vec{r}} \mathrm{d}^3\vec{r} \tag{11}$$

$$\rho(\vec{r}) = \mathcal{F}^{-1}(K(\vec{k})) \sim \int_{-\infty}^{\infty} K(\vec{k}) e^{-\mathrm{i}\vec{k}\vec{r}} \mathrm{d}^3\vec{k} \tag{12}$$

$\mathcal{F}^{-1}$ here represents the inverse Fourier transform. In the implementation as digital scanning process, this continuous description, of course, has to be translated into a discrete formulation. Finite borders of the integral then define the maximally perceivable resolution and summation of discrete values instead of integration means that the acquired window in real-space – the "field of view" – is limited.

1.3.3 Image contrast and contrast agents

It is possible to generate a variety of contrasts with MRI. Additionally to the signal strength given by the concentration of water or fat, the relaxation parameters T_1 and T_2 have a strong influence on the imaged intensity. They are dependent on the chemical environment, as the respective proton spins interact with each other.[34] Thus, in medical imaging one aims to introduce contrast based on the imaging purpose via adapted imaging protocols.

Generally, the relaxation effect (T_1) in longitudinal and the dephasing (T_2) in transverse direction of $\vec{M}_0$ is exploited by use of a combination of

RF pulses and the previously described magnetic gradients in a manner similar to the following: The excited spins respond on the RF pulse with an echo, when a rephasing happens after their dephasing. This can be achieved, firstly, by additional RF pulses or, secondly, by forcing rephasing with additional gradients. An example for the first method is the use of 90° pulses in combination with subsequent 180° pulses. Here, the spin dephasing is inverted via the 180° pulse, so a rephasing appears at the echo time (T_E) of 2 times the time between the 90° and the 180° pulse. The second method first accelerates dephasing of the spins by a dephasing gradient, and, analogously a reversely strong rephasing gradient forces an echo. MR sequences using the first principle are called spin-echo sequences, whereas sequences incorporating the second method are called gradient-echo sequences.

For T_2 weighted sequences one waits for the spins to be nearly relaxed in longitudinal direction (long T_E). Short repetition times between excitations (T_R) and short T_E, thus, lead to T_1 weighted images. Gradient-echo sequences can be accelerated comparably easy by quick switching of the gradients and adjustment of their strength. As this work deals mainly with T_1-related effects in the region of the *moving* heart, the fast gradient-echo sequence is particularly well-suited to serve as a basis for it (see 1.3.4).

To enhance the image contrast in MRI, contrast agents can be applied additionally. Widely used and relevant to this work is gadolinium. It is mostly applied as non-specific contrast agent for a broad range of MR exams.[6] To describe the relaxation behavior, Ionel Solomon developed a model for two spins in laboratory conditions.[44] A strong dependency on the gyromagnetic ratio is derivable from it, which for two *different* particles separates into

$$T_1 \propto \gamma_{p1}^{-2} \cdot \gamma_{p2}^{-2}. \tag{13}$$

Gadolinium is extremely paramagnetic with 7 unpaired electrons in the 4f shell and as a consequence has a 600 times larger γ than the proton. This means that regions containing gadolinium have a significantly decreased T_1, resulting in strong image contrast in T_1 weighted MR images. Gadolinium is

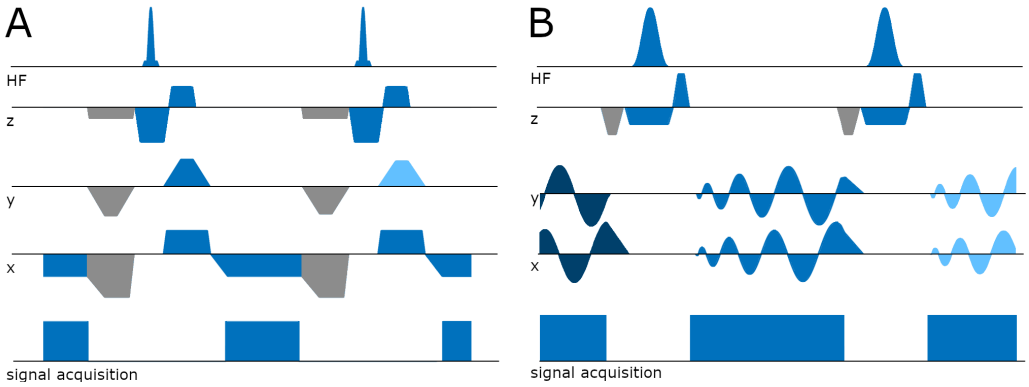

Figure 2: Spoiled gradient echo sequence (A:) with Cartesian k-space trajectory and (B:) with spiral k-space trajectory. Changing elements with respect to the subsequent repetition are depicted in a different shade of blue. Elements merely used for spoiling the transverse magnetization are depicted in grey and not further explained.
HF: exciting radio frequency pulse z: slice selection gradient y: phase encoding gradient x: frequency encoding gradient

applied as chelate, i. e. surrounded by a ligand molecule to protect the body from its toxicity.

1.3.4 MR sequence

This section goes into further detail regarding the gradient echo sequences used in this work (illustration in figure 2). Traditionally in MRI, the k-space is acquired in a Cartesian manner. In this case, one can consider the magnetic gradients to be applied separately in the three spatial directions as slice selection, phase encoding, and frequency encoding gradients. Either of the three possible MRI gradient directions can be assigned to the slice selection, resulting in imaging in the transverse, the sagittal, or in the coronal plane of the subject.

Firstly, the slice selection gradient is applied *during* excitation. This means that just one slice in real-space resonates with the frequency of the incoming radiation. The slice thickness is defined via selection of the bandwidth.

As a next step, a phase encoding gradient is run. While this gradient is

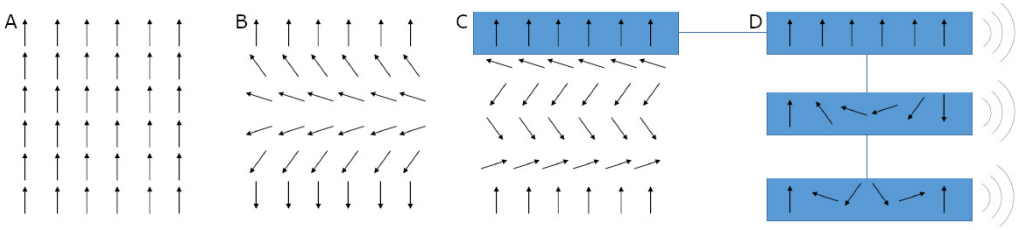

Figure 3: Sketch of the spins belonging to one slice during a Cartesian read-out. A-C: Three “vertical" gradient strengths result in three different phase encodings. D: A “horizontal" gradient causes the frequency encoding. Note that not the signal of spins belonging to just one real-space point is measured, but a spatial frequency, respectively, is being impressed on the spins in both slice directions.

active, the spins rotate with varied angular velocity for a defined time period (figure 3). Therefore, spins with a certain spatial distance in phase encoding direction will be in phase after the application. With this, one k-space line (one spatial frequency to acquire) is selected.

In a last step, an additional gradient varies the frequency of the spins *while* the signal is being recorded. This step is called frequency encoding. The spin runs through all frequencies from one end of the (discrete and limited) spectrum to the other, which means that the selected k-space line has been read. The measured k-space line is not a line in real-space, but it represents a 2-dimensional regular pattern of parallel waves.

To receive an image in the Cartesian acquisition pattern, one has to acquire the spatial frequency steps in both planar directions from zero up to the desired image resolution and then perform the inverse Fourier transform.

1.3.5 Non-Cartesian imaging

Non-Cartesian trajectories The path which the k-space scanning takes does not necessarily have to be in the pattern of parallel lines. Instead, arbitrarily chosen paths are feasible.[10] With the two encoding gradients run simultaneously as exemplarily shown in figure 2 B, a spiral trajectory can be marked. This particular sequence yields a spiral which starts in the k-space center and continuously moves outwards (fig. 4).

A spiral trajectory has the advantage of avoiding fast turning points.

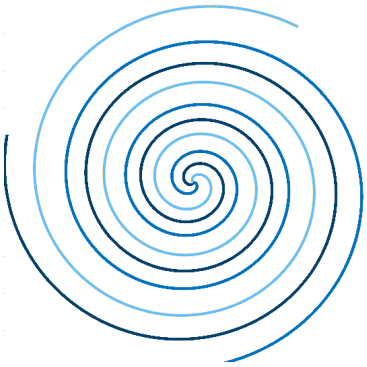

Figure 4: Three arms of a spiral k-space trajectory. The center of k-space is sampled with every spiral read-out (with a Cartesian sampling pattern just once).

Also, no time is lost by phase encoding before the actual read-out. Therefore, spiral and other trajectories can be designed to be more efficient. Additionally to the increased sampling rate, non-Cartesian imaging offers beneficial conditions for acceleration via undersampling for some reconstruction techniques (see subsection 1.3.6). These are based on irregular sampling to ensure the incoherence of appearing undersampling artifacts.[18] A third advantage can be exploited when covering the k-space center regularly instead of just once.[29] The consequence of this redundant sampling is that coarse changes are not missed, which decreases imaging artifacts caused by motion.

Trajectory correction Due to MR scanner system imperfections and eddy-currents,[22] gradient outputs deviate regarding the nominal magnitude and phase in a low-pass like fashion. Unfortunately, this effect becomes especially visible for non-Cartesian trajectories,[41] which contain a lot of gradient changes. To compensate the errors appearing in the MR sequences with non-Cartesian sampling, all output gradients used in this work have been corrected by an automatic pre-emphasis.[46] To this end the scanner specific gradient system transfer function (GSTF) was measured. It is the function of the change in the output gradient over the played out frequency range. Its inverse was used to correct the input as follows.[13]

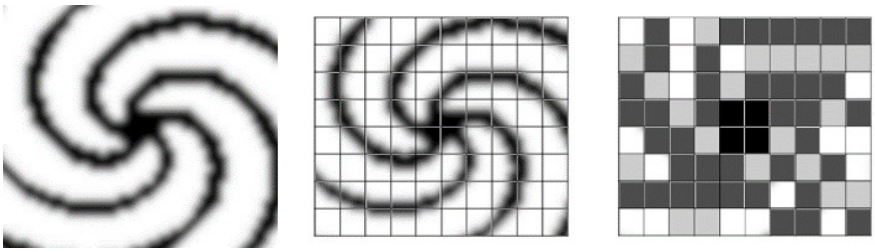

Figure 5: Image illustrating k-space gridding, e. g. using GROG.

$$g_{i,cor}(t) = \mathcal{F}^{-1}\left(\mathcal{F}(g_i(t)) \cdot \mathrm{GSTF}_{i,i}^{-1}(f)\right), \tag{14}$$

$i \in \{\mathrm{x}, \mathrm{y}, \mathrm{z}\}$ is representing the three gradient directions, t and f the dependency on time or frequency and $\mathcal{F}$ is the Fourier transform. This way, the actually intended waveform is played out, yielding the expected k-space trajectory.

Data matrix To create an image matrix from a spiral MR acquisition, recorded signal intensities have to be transferred to the Cartesian grid. One common approach to do so is the non-uniform fast Fourier transform (NUFFT), which is the direct way to translate non-Cartesian k-space data into Cartesian real-space. Another approach is actually calculating Cartesian k-space grid values that resemble the measured data, and then using standard 2-dimensional fast Fourier transform (fig. 5).[21] For example, this can be performed via GRAPPA-operator gridding (GROG[42]). The GROG approach is well suited for iterative algorithms such as the following work, where the gridded k-space data is being used repetitively.

GROG is a two step process: An operator is calculated from the used trajectory[43] together with the sampled data. After that, the operator is used to find the change in a k-space intensity for a given small translational difference (a, b). The basis for GROG is an approximation to shifting k-space points via adequate matrix multiplication.

$$S(k_x + a, k_y + b) = G_x^a \times G_y^b \times S(k_x, k_y), \tag{15}$$

where S is the k-space signal and G means the shift operators in the orthogonal directions. This way, the non-Cartesian samples determine the values of their nearest Cartesian matrix location. If there are multiple samples which have the same Cartesian next neighbor, the value is averaged from the respective results.

1.3.6 Redundancy in MRI

In dynamic MRI, the imaged object stays the same with the exception of some moving elements. This can be utilized for imaging purposes. Furthermore, the motion is often limited to a defined image region and quasi-periodical. As traditional Cartesian MRI is slow compared with the imaged physiological processes, many imaging techniques have been developed that use prior knowledge to make up for sampling less data than would actually be necessary for an artifact-free image. To illustrate this, one can imagine a signal course that is known to be linear in all pixels over time. In this example, just two samples suffice to reconstruct the signal course for all points in time, or, in other words, the acceleration would have been achieved by exploiting redundancy by applying a linear model.[48]

Compressed sensing A powerful way to exploit the redundancy of dynamic acquisitions is summarized by the term 'compressed sensing'. Compressed sensing[15] is based on the idea of image compression, i. e. an image can be cleverly represented using fewer information without perceivable loss of quality. Simultaneously, this means that the necessary amount of measured samples suffices as long as the perception limit of the resulting image is being met. The three requirements for compressed sensing are

- the possibility to represent the data sparsely, i. e. in a space that is zero with just a few exceptions,

- incoherently sampled data in such a way that undersampling artifacts appear noise-like in the sparse representation,
- a reconstruction in the basic form of a minimization

$$\text{argmin}_m \quad ||y - \text{F}m||_\text{a} + \lambda||\text{T}m||_\text{b}, \tag{16}$$

with a data consistency term in combination with the sparsity enforcement. Here, m is the reconstructed image, (in the context of MRI) F means the coil separation and subsequent Fourier transform, to conform with the measured k-space samples y. T is the transformation into the sparse representation and λ an adjustable regularization parameter, while data consistency and sparsity are contained in the form of a certain norm (here denoted with a, b).

Otazo et al. proposed a reconstruction for dynamic data, where the image m is separated into a low-rank and a sparse component $(L + S)$,[37] where basically two filter steps take the role of the sparsity transform:

$$\text{argmin}_{L,S} \quad ||y - \text{F}(L + S)||_2^2 + \lambda_L||L||_* + \lambda_S||\text{T}S||_1 \tag{17}$$

Here, 1, 2 and * denote the l_1-, the l_2-, and the nuclear norm. Minimizing the nuclear norm, i. e. the sum of singular values, is identical with ensuring a low rank and thus a low variation over time. On the other hand, the l_1-term, i. e. sum of absolute values, of the Fourier transform of the sparse part in temporal direction (T) keeps the change of details within well-defined limits. This separation using additive separation into background (L) and rapidly changing elements (S) was already applied successfully multiple times in dynamic MR imaging.[9,13,37]

1.3.7 Motion correction

Another topic that was important in this work and deals with the processing of dynamic MR data is motion correction. For some medical evaluation

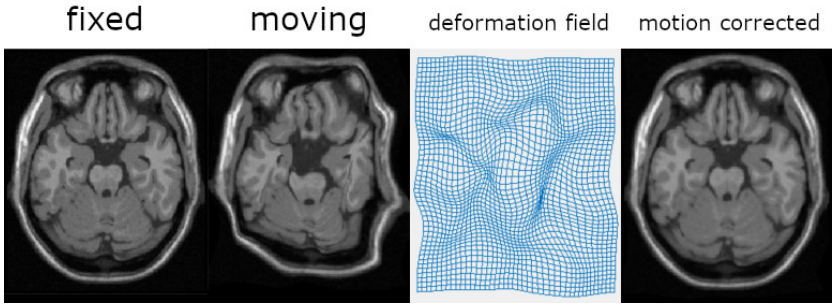

Figure 6: The image “fixed" serves as reference for the calculation of a deformation field with respect to the image “moving", which was distorted on purpose. Knowing the deformation, one can correct most of the artificial motion. The shown registration is performed by the medical image registration toolbox MIRT.[35]

techniques, static images or image series from moving organs are crucial. Examples for this are the quantification of lung function or blood flow in the heart. Therefore, motion correction software is a permanent aspect of MRI research. While respiratory motion can often be approximated as shift of the whole imaged region and rigid transformations can be used to correct for motion, non-rigid motion correction is necessary to transition from an image sequence of a beating to one of a still heart. This, firstly, requires the approximation of tissue flexibility. The other necessary part of a motion correction algorithm is a similarity function, which assigns a similarity score to the images. Finally, the motion correction needs an optimization algorithm to propagate from local solutions to, ideally, the global similarity maximum.[23]

Usually, the registration of an image pair results in a vector field representing the motion in between the two images within the set transformation limits. Applying the vector field on the second image referred to as “moving" warps it to resemble the shape of the object on the first image referred to as “fixed" (see example fig. 6). That way, assuming an image series of different cardiac phases, if one image is set as fixed and all other images of the series as moving, application results in a motion corrected image series, i. e. the heart should appear static.

2 Cardiovascular MRI

Cardiac MR (CMR) exams comprise a broad spectrum of diagnostically relevant measurements. Ventricle volumes as well as the blood flow itself deliver meaningful information about the cardiac function. Additionally, MR sequences can be used to characterize the myocardial tissue, e. g. to recognize inflammation, scarring, or substance accumulation.[20] Contrast agents can help to suppress or enhance local MR signal intensities, e. g. the blood pool, acute infarction, scar tissue, and fibroses. Three of the commonly applied exams, which are strongly related to this work, are cine imaging for evaluation of the cardiac function, delayed gadolinium enhancement imaging, which exploits the use of contrast agent, and T_1 mapping. (An attempt for standardizing the cardiovascular MR exam is referenced.[28])

2.1 Cine structural and functional imaging

Cine MRI yields a slice-wise loop movie of the heart.[9] Typically, its gradient-echo acquisition is run as balanced steady-state free precession (bSSFP) sequence. Allowing free spin precession in contrast to spoiling in a spoiled gradient echo sequence, results in higher signal yield in combination with short repetition times. The cine acquisition traditionally constitutes a segmented measurement, which means that the sampling of the k-space of each image frame is split into multiple non-successive part acquisitions.[7] The k-space lines are assigned to the correct movie frame based on the cardiac phase. The latter is either determined retrospectively by dividing the ECG signal from “R" wave to the next “R" wave into equal parts (see figure 7) or prospectively by triggering the acquisition with the “R" wave and assuming a steady heartbeat. The defined number of separate phases (segments) varies in the range of 10 to 30 frames (25 frames in the shown example fig. 8).

2.2 Delayed gadolinium enhancement imaging

The following section describes the gold standard for the assessment of viability of myocardial tissue. The relevance of this part of the CMR exam is

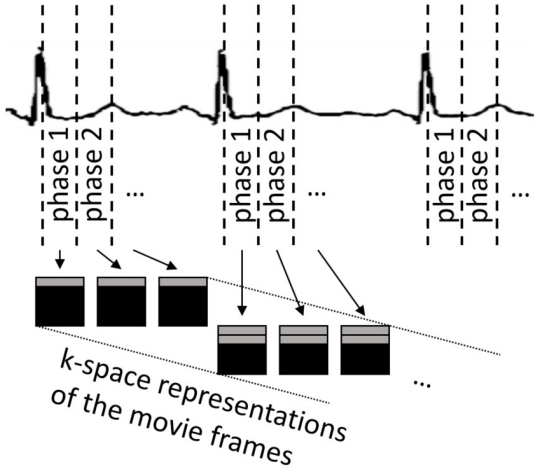

Figure 7: Segmentation of the data in a cine measurement. The ECG-signal serves as basis for the assignment of the k-space lines by marking the first cardiac phases, respectively, with the prominent “R" wave.

based on the fact that viable tissue, in contrast to nonviable tissue, is either functional or likely to recover and regain functionality.[50] As described in 1.3.3, it is possible to influence the T_1 dependent signal intensity via infusion of a contrast agent. Most of the contrast agents containing gadolinium are not target-specific and stay in the blood and extracellular fluid until renal elimination.[25] Delayed gadolinium enhancement (LGE) is well-suited for assessing viability, as scarred, necrotic, or wounded tissue has significantly altered durations for the wash-in and wash-out of the contrast agent compared with healthy tissue (see fig. 9).

An acute myocardial infarction shows an enhanced signal due to prolonged wash-out because of an increased contrast agent containing volume in the muscle. The reason for this is the disruption of membranes of necrotic cells in acute infarctions. Chronic infarctions, on the other hand, are typically associated with myocardial thinning, where a prolonged wash-out is associated with the loss of contractibility.[50] An example for an LGE image, acquired after a myocardial infarction occurred, is shown in figure 10. Subsequently to a delay of 10 minutes after contrast agent application, the gadolinium containing agent has passed through the main part of the muscle,

Figure 8: Clinically acquired bSSFP cine of the patient, whose contrast enhanced images are also shown in figure 29. The single frames of the sequence are shown row by row.

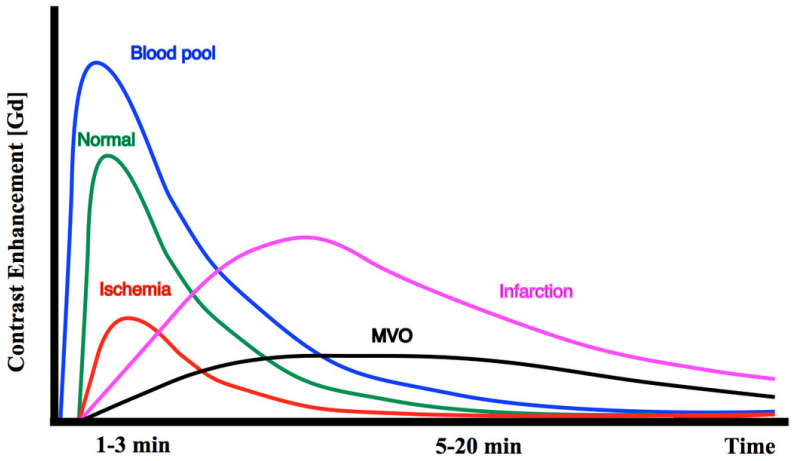

Figure 9: Courses of contrast agent concentrations in normal and affected myocardium. (MVO: microvascular obstruction)[14]

but still lingers in the damaged or scarred tissue. Using magnetization inversion preparation in the MR sequence, the signal of the affected myocardium recovers quicker, and it appears bright, while healthy myocardium is still dark.[26]

The contrast agent flow varies between every patient and has strong influence on the signal recovery duration. Thus, the point in time after the inversion (TI) of maximum contrast is commonly determined on-site by the examiner using a TI-scout MR sequence. It represents a trial run through a range of possible TIs, which allows to pick the best of multiple low resolution images reconstructed on-the-fly. To acquire a fully sampled LGE image, the segmented measurement is then performed around this chosen TI. The ECG signal here triggers the inversion to synchronize cardiac phase and TI for each segment.

Because MR yields complex-valued data, two main representations are established in imaging. The first way is to display the absolute values, the second is to turn the data by the complex phase onto the real axis, so the sign is not lost. To be able to store the image in the common DICOM (= Digital Imaging and Communications in Medicine) format, positive values are required, which is the reason why an offset of the lowest value ($\min(s)$) is

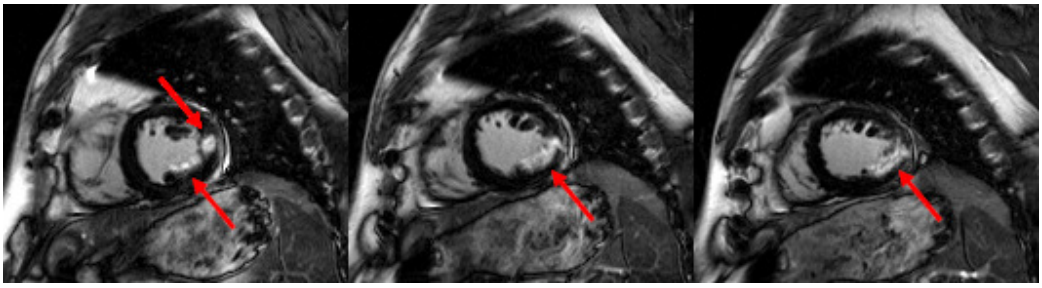

Figure 10: Three adjacent slices of a clinical LGE exam of a patient with acute myocardial infarction (figure belongs to same acquisition as fig. 33). Affected tissue appears bright because of delayed enhancement (red arrows) induced by the contrast agent, which contains gadolinium.

subsequently added. The first option is called magnitude, the second phase-sensitive (PSIR) representation.

2.3 T_1 mapping

T_1 mapping is part of the field of quantitative MRI. Here, the depicted pixel values are the physical relaxation parameter itself. This is done by capturing the magnetization course, e. g. by using magnetization inversion or saturation preparations and subsequent acquisitions. An image in which every voxel represents the corresponding T_1 value is called T_1 map.

In case of a gradient echo sequence, the relaxation course is disturbed by every small excitation depending on the flip angle. Firstly, this means a faster relaxation into a maximal magnetization level, secondly, it reaches just a steady state M_∞ instead of M_0. The basic non-perturbed magnetization course after inversion preparation is

$$M(t) = M_0 - 2M_0 \exp\left(-\frac{t}{T_1}\right). \tag{18}$$

The perturbation by the flip angle α and the exponential decay until the next repetition T_R, respectively, amounts[11] to

- $M \longrightarrow M\cos(\alpha)$ and

- $M \longrightarrow M_0 + (M - M_0)\exp(-T_R/T_1)$,

meaning one increment until the next perturbation is

$$M_{\mathrm{i}+1} = M_0 + (M_{\mathrm{i}}\cos(\alpha) - M_0)\exp\left(-\frac{T_R}{T_1}\right). \tag{19}$$

The equation (19) for M_∞ yields the factor for the decreased steady-state magnetization of the acquisition as

$$\frac{M_\infty}{M_0} = \frac{1-\exp(-T_R/T_1)}{1-\cos(\alpha)\exp(-T_R/T_1)}. \tag{20}$$

Using the effective relaxation time T_1^*,

$$\frac{1}{T_1^*} = \frac{1}{T_1} - \frac{1}{T_R}\ln(\cos(\alpha)), \tag{21}$$

the term describing the steady-state magnetization (eq. 20) becomes

$$\frac{M_\infty}{M_0} = \frac{1-\exp(-T_R/T_1)}{1-\exp(-T_R/T_1^*)}. \tag{22}$$

Implying short T_R (i. e. $\exp(-T_R/T_1) \approx 1 - (T_R/T_1)$), this leads to the traditional approximation used for T_1 determination,[11]

$$T_1 = \frac{M_0}{M_\infty}\cdot T_1^*, \tag{23}$$

and the adapted relaxation curve is

$$M(t) = M_\infty - (M_0 + M_\infty)\exp\left(-\frac{t}{T_1^*}\right). \tag{24}$$

An exemplary T_1 map is shown in figure 11. For simplification 100 %

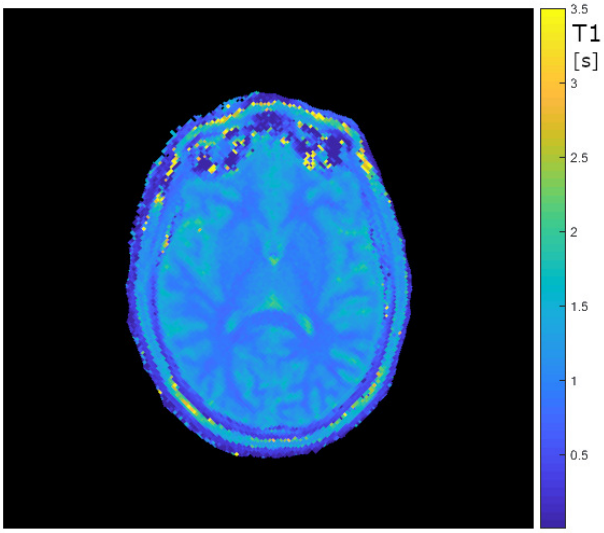

Figure 11: T_1 map of one slice of the human brain, acquired with a spoiled gradient-echo sequence.

inversion efficiency was assumed, so the ground state equals the inverted magnetization $M_0 = M(t = 0)$. M_∞ and T_1^* can be determined by a least-squares fit.

3 Methods

3.1 MOCO-MAP

Already published in 2013,[47] model-based acceleration of parameter mapping (MAP) is a way to reconstruct undersampled saturation recovery data and to generate T_1 maps of the human brain. Because of the signal change during the relaxation process, the acquired data has to be gridded (1.3.5) to adequately small temporal bins to avoid information loss due to averaging. Consequently, the imaged object is heavily undersampled. MAP supplies the missing data via exponential relaxation model in real-space.

To make use of MAP in cardiac imaging the only missing component is principally motion correction (MOCO). This way, the signal course of the static myocardial area allows analogous image reconstruction.[55] Unfortunately, current algorithms for the calculation of motion fields, such as MIRT,[35] elastix[27] and VoxelMorph[1] turn out to be dependent on many parameters. In the latter case, the motion correction accuracy is additionally dependent on the similarity to a training data set for machine learning. Because of this complexity, these algorithms can cause blurring or even image distortion. Methods not relying on image registration (e. g. sec. 3.2), on the other hand, are often more accurate and tend to be faster. However, for scientific completeness and the opportunity to pass on ideas, the method of MOCO-MAP and its results shall be described in the following. As exponential model and motion correction make up the core of MOCO-MAP, they will be explained first.

3.1.1 MAP

The model used in MAP[47] is based on the physical relaxation, which is already described in section 2.3. Assuming correctness of equation 24, which is commonly used in T_1 mapping via gradient-echo sequences, M_0, M_∞ and T_1^* fully describe the signal course of $M(t)$. To find these parameters, the MAP algorithm iteratively uses three-parameter fitting in real-space and corrects

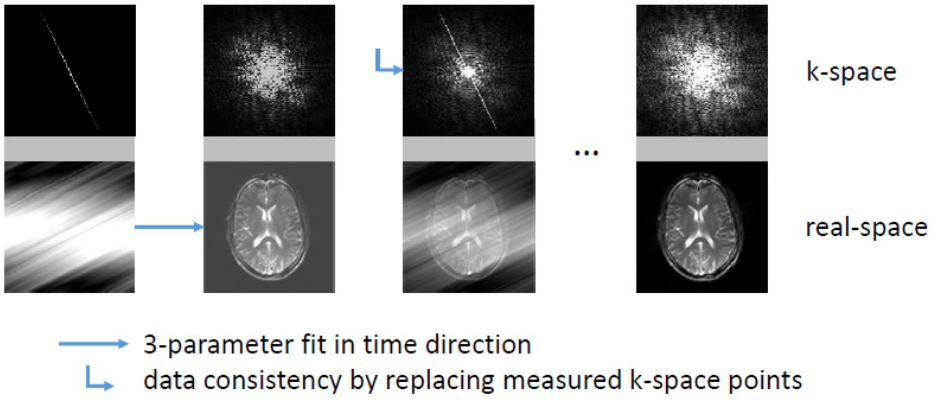

Figure 12: Working out the true magnetization course by alternation between 3-parameter fit and reinsertion of the originally measured data. The algorithm converges (indicated with '...') corresponding to the fully sampled equivalent. Note that these images represent a time series of 2D k-space/real-space arrays, respectively.[47]

the interim result by reinserting the measured data samples in k-space (see fig. 12). Taking turns in this process each fit forces the model onto the data and then the reset of the actually measured k-space points restores consistency with what is known about the object.

One precondition for MAP to work properly is a still measured object. Otherwise blurring is introduced to the the motion afflicted image region.

3.1.2 MOCO

The motion correction attempts for the presented inversion recovery acquisitions are discussed in the following. One of the main difficulties of motion correction (1.3.7) of IR data is the fact that not just the imaged object moves, but also the signal intensity distribution changes over time. This means that, unlike for motion correction e. g. applied in cine imaging, consecutive images have to be adapted to fit for registration. Although VoxelMorph[1] has been tested, all image registrations of the presented results were performed via MATLAB toolbox MIRT,[35] which uses a gradient-based optimization, a curvature-based regularization, and a hierarchical approach to register on

multiple resolution levels.

Pseudo heartbeat The original MOCO-MAP approach[55] to tackle the problem of signal change due to relaxation is to use a prolonged measurement in breath-hold to gather sufficient image data during the fully recovered magnetization state.[54] This acquired data of full cardiac cycles without signal change enables image registration. Further refinement can be achieved by averaging multiple acquired heartbeats into one cine depiction and, for example, by using compressed sensing to exploit the redundancy of the dynamic image series (1.3.6). Image registration of this cine (= pseudo heartbeat) results in a vector field representing the repeated motion of the heart. Together with the ECG, the motion field can then be interpolated and applied[†] according to the respective cardiac phase for the whole data set. Thus, correct ECG recording is a precondition for an accurate application, and patient motion is neglected. Otherwise, motion correction is either applied in the wrong time or region.

Iterative MOCO To investigate a more robust way to incorporate the motion correction, iterative motion correction was introduced. Here, the reference for the registration is not based on a prolonged acquisition and a reconstruction step, which precedes the main iterations, but on the data within the algorithm itself. To do this, a frame-by-frame registration of the moving image series onto the exponential model fit series is used. This is possible, because the fit represents a (fixed) average of the image series while the magnetization change is maintained (see fig. 13).

To eliminate random registration errors and to prevent undersampling artifacts to be interpreted as motion, the motion field can be median filtered in temporal direction.

Assuming well-adjusted image registration, the iterative MOCO concept

[†]The specific tools to apply the motion field depend on the used software. By switching 'moving' and 'fixed' and registering twice, the motion field and its reverse can be found in any case. With "application of a motion field", I denote both: motion correction and the restoration of motion. To avoid consecutive faults with iterative methods, I recommend inverting the motion field as exactly as possible.

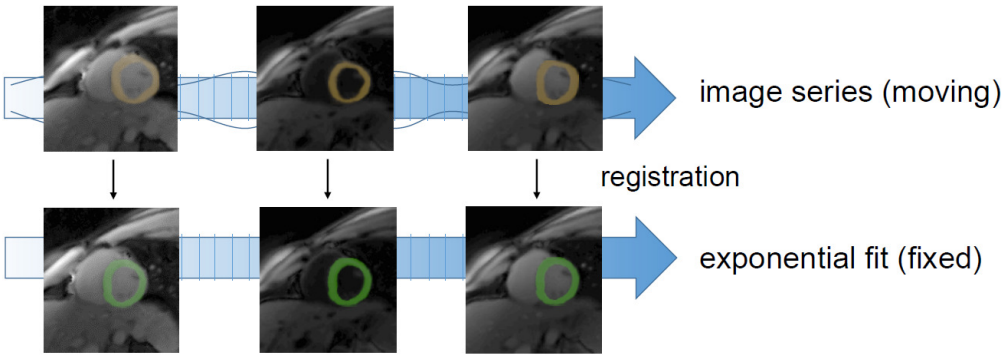

Figure 13: Frame-by-frame registration using the exponential fit as a reference to tackle the problem of changing contrast. The moving left-ventricular myocardium is highlighted in yellow, the fixed in green.

is expected to have three major benefits. One is the decreased measurement time, which is just limited by the Nyquist criterion with respect to the full acquisition length. Another is an increased robustness towards patient motion. Finally, it is independent from the ECG signal recording.

3.1.3 MOCO-MAP algorithm

This section illuminates the detailed steps of the MOCO-MAP implementation. In the iterative MOCO-MAP reconstruction, first, the model is applied on the motion corrected image series, and then, the consistency with the measured data is enforced in k-space. An overview of the algorithm is given in figure 14, the single steps are:

- The measured signal intensities are given in the order of acquisition, their k-space location can be assigned by the set sampling pattern.
- To generate a pixel-based k-space image, the values and the sampling pattern are combined using GROG (see subsection 1.3.5).
- The inverse Fourier transform yields an image series in real-space. This raw series has undersampling artifacts: blurry with bent stripe-like intensity fluctuations.

- To allow approximation via an exponential model, a real-valued image array is generated. As both (complex) receiver channels measure the same object, one can assume that the dependency between real and imaginary part is approximately linear and the inversion of the magnetization causes the signal to cross the origin of the complex plane. This means that the complex phase at the location x can be estimated by

$$\varphi(x) = \text{median}_{t=t_n}^{t_N} \left[\angle(s(x,t)) \right], \tag{25}$$

  where $\angle$ denotes the complex phase, s the complex signal measured by one coil, and t_n until t_N acquisition points in time on just one side of the zero-crossing. The real-valued signal (s_r) is

$$s_r(x,t) = \text{real}\left[s(x,t) \cdot \exp(-\text{i}\varphi(x)) \right]. \tag{26}$$

  After this phase correction the signal of all single coils ($s_{r,i}$) can be combined to S_r by the sum-of-squares method as

$$S_r(x,t) = \text{sign}(\sigma) \cdot \sqrt{|\sigma|}, \tag{27}$$

$$\sigma(x,t) = \sum_i \text{sign}(s_{r,i}) \cdot s_{r,i}^2, \tag{28}$$

  to further preserve the signal sign.

- For the resulting image series, one of the proposed motion correction approaches (3.1.2) can be applied.

- A pixel-wise mono-exponential least-squares fit (eq. (24)) in temporal direction now traces the signal course of each voxel, respectively.

- After the motion field is reapplied, image series and measurement match again.

- To return to the complex and coil-combined version of the image, the phase map $\varphi(x)$ from the phase correction step and externally determined coil maps can be used. Alternatively, a pixel-wise linear fit can

serve to find the complex factor for each coil that connects the new real image with the coil-separated image from the previous iteration step best.

- After a Fourier transform the k-space is now filled with values conforming to the exponential model and is compared with the original array containing the measurement data. All k-space coordinates with measured (= non-zero) points replace the approximate values yielding a version, which is consistent with the samples.

- With the improved k-space the next iteration starts by again switching to real-space.

As stopping criterion, one can set a limit for the difference of any intermediate image and its version in the previous iteration. The number of iterations until the image converges depends on the choice of how many acquired spirals are binned, i. e. the set temporal resolution. MOCO-MAP with a temporal resolution of about 50 ms converges after few iterations, but the reconstruction is still very time consuming (around one day for one reconstructed 2D image series). Usually after 8-10 iterations no significant differences with respect to the previous iteration are visible.

3.1.4 Subject study

A spoiled gradient echo IR sequence with spiral trajectory was used (TR: 5.0 ms – 5.6 ms, flip angle: 10 °, in-plane resolution of $1.51 \times 1.51\,\mathrm{mm}^2 - 1.42 \times 1.42\,\mathrm{mm}^2$ and a slice thickness of 5 mm), equipped with a GSTF-based gradient correction (see 1.3.5). Data was sampled for 5.0 s – 10.3 s in breath-hold from volunteers and patients, one mid-ventricular short-axis slice was acquired.

The conducted study was approved by the ethics committee of the University of Würzburg (submission date: 08.04.2019, corresponding code: 90/19-sc). An inclusion criterion for the patients in the study was a clinically induced cardiac MRI examination with the use of contrast agent (intravenous

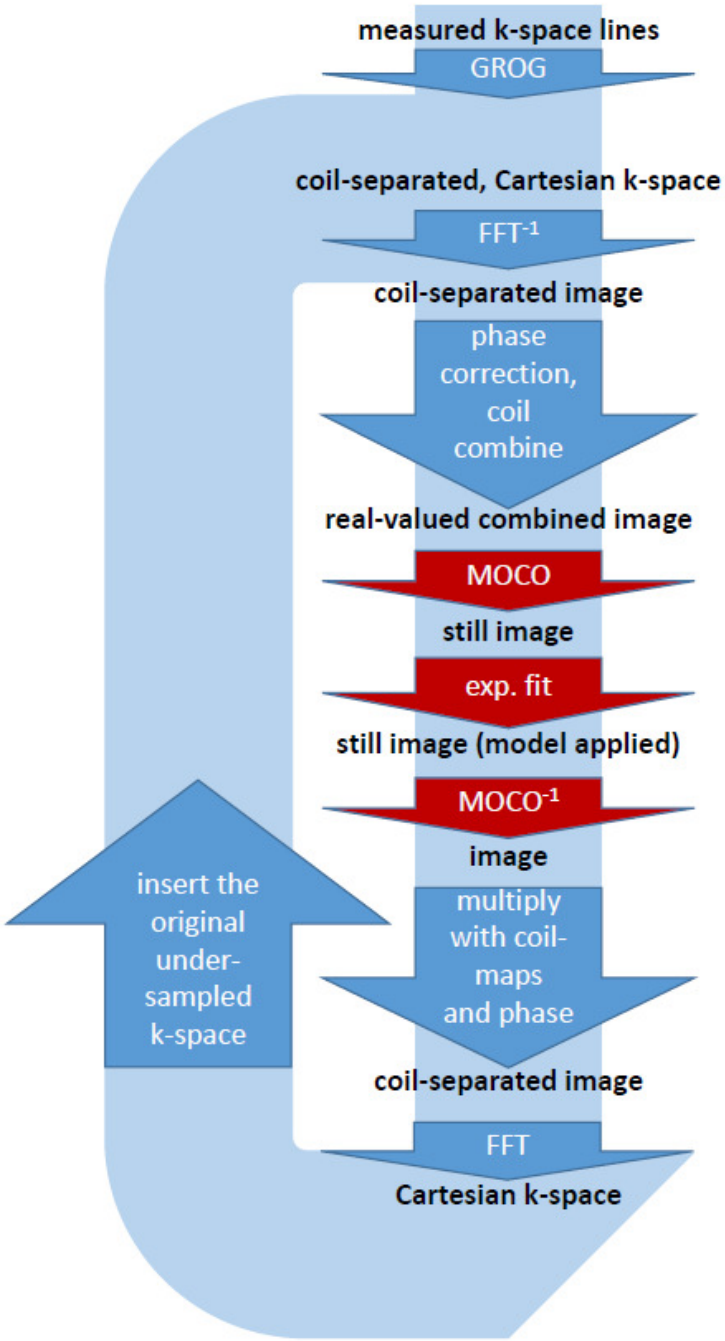

Figure 14: MOCO-MAP processing steps. The core operations – motion correction and application of the exponential model – are shown in red.

application of 0.4 ml/kg body weight of Dotagraf [Jenapharm, Jena, Germany]). Written informed consent was obtained from all subjects. For reference LGE bSSFP exams were performed, with TE: 1.54 ms, TR: 3.8 ms, flip angle: 40 °, breath-hold duration: 10–12 s, 5 IR preparations, in-plane resolution of $1.3 \times 1.3 \times \text{mm}^2$, slice thickness of 8 mm and TI: 280–340 ms. The MOCO-MAP acquisitions were scheduled subsequent to the completed reference exam, i. e. 20–30 minutes after contrast agent application.

3.2 IR-CRISPI

When finding a suitable reconstruction method, it is crucial to be aware of the limiting factor, which is dominantly responsible for loss in image quality. Moreover, in radial and 3D sampling, undersampling often leads to severe stripe-like undersampling artifacts. For the proposed 2D spiral real-time sampling,[13] the amount of samples per time segment is closer to full sampling. In this case undersampling manifests mainly in blurring, which is less obstructive for the reconstruction of the image. As a consequence, exploitation of the redundancy can be achieved by a softer constraint. In the proposed method, inversion recovery cardiac real-time imaging using a spiral trajectory (IR-CRISPI),[39] it is achieved by separation into low-rank plus sparse[37] part, which is related to compressed sensing.

3.2.1 Conception

Preceding this work, the low-rank plus sparse[37] reconstruction could already be successfully applied (see 1.3.6) on spiral cine acquisitions.[13] Due to the appearance of low-signal periods during zero crossing of the signal course, the reconstruction was then augmented with an additional wavelet constraint.[52] This way, the increased effective noise level is reduced. The modified minimization problem[39] can be formulated as

$$\text{argmin}_{L,S} \quad ||y - \text{F}(L+S)||_2^2 + \lambda_L ||L||_* + \lambda_S ||\text{T}S||_1 + \lambda_W ||\text{W}(L+S)||_1. \tag{29}$$

Here, the measured k-space data is y, low-rank and sparse part are L and S. Transforms are the spatial Fourier transform combined with the coil-separating and sampling operator F, the Fourier transform in time domain acting as sparsifying transform T and the wavelet transform W. The norms denoted with 1, 2 and * are the l_1, l_2 and the nuclear norm, respectively. Regularization terms are accompanied by the respective parameters $\lambda_{L/S/W}$.

With focus on an optimized application and evaluation of IR-CRISPI, it was designed to gather functional (constant contrast) and viability (signal recovery) information in a single measurement. The reconstructed data sets were separated afterwards, to firstly deliver cine-like movies, which are manually synchronized at the second heartbeat to improve volume assessment. Secondly, a novel data set was generated for an LGE image series covering not only one point in time but the signal recovery, which permits to retrospectively search for the optimal contrast between healthy and diseased myocardium.

3.2.2 IR-CRISPI algorithm

The IR-CRISPI algorithm (illustrated in fig. 15) works analogous to MOCO-MAP (see 3.1.3), but instead of

- real-valued data, it is possible to work with the original complex-valued data, which means the phase correction step can be omitted.
- the exponential fit, the steadier image content is represented by the low-rank part, i. e. a soft-threshold of the image minus sparse part of the last iteration is performed at λ_L: 0.01.
- the motion field via image registration, the motion is maintained and noise-filtered in the sparse part S, initialized with 0. It is the image minus the newly updated low-rank part. Filtering via soft-threshold in time-domain (at λ_S: 0.05) acts as sparsifying transform.

Noise suppression is performed subsequently to the determination of L and S by wavelet filtering $L + S$ at a cut-off (λ_W) of 0.003.

By design, these changes prevent artifact generation due to deviations with respect to exponential behavior, regardless whether these arise from flaws in the phase correction, suboptimally regularized exponential fit or partial volume effects. Additionally, image distortion or extra blurring due to image registration is avoided, while the reconstruction is accelerated immensely. Least-squares fits and image registrations take up significantly more time in comparison to fast Fourier transforms, leaving the gridding procedure as slowest single operation.

3.2.3 Patient study

A spoiled gradient echo IR sequence with spiral trajectory was used (TR: 5.0 ms, flip angle: 12 °, in-plane resolution of $1.54 \times 1.54\,\mathrm{mm}^2 - 1.42 \times 1.42\,\mathrm{mm}^2$ and a slice thickness of 8 mm), equipped with a GSTF-based gradient correction (see 1.3.5). Data was sampled for 5.0 s – 10.3 s in breath-hold of the subjects, one mid-ventricular short-axis slice was acquired.

A patient study including 10 patients after contrast agent application (intravenous application of 0.4 ml/kg body weight of Dotagraf [Jenapharm, Jena, Germany]) was conducted. The conducted study was approved by the ethics committee of the University of Würzburg (submission date: 08.04.2019, corresponding code: 90/19-sc). Written informed consent was obtained from all subjects. As references for functional imaging, prior to the contrast agent application, cine images were acquired in the course of the medically indicated standard exam (TE: 1.41 ms – 1.51 ms, TR: 3.19 ms – 3.48 ms, flip angle: 42 ° – 50 °, in-plane resolution: $1.44 \times 1.44\,\mathrm{mm}^2 - 1.26 \times 1.26\,\mathrm{mm}^2$, slice thickness: 8 mm, temporal resolution 38.3 ms – 40.9 ms, performed in breath-hold over 12 heartbeats). Additionally, LGE reference images were acquired (TE: 1.54 ms, TR: 3.8 ms, flip angle: 40 °, breath-hold duration: 10 – 12 s, 5 IR preparations, resolution of $1.3 \times 1.3\,\mathrm{mm}^2$, slice thickness: 8 mm and TI: 280 ms – 340 ms). The IR-CRISPI acquisitions were scheduled 8–9 minutes after contrast agent application and directly before the LGE reference exams.

Evaluation To receive reliable values for the quantitative functional measures of end-diastolic volume (EDV), end-systolic volume (ESV), ejection

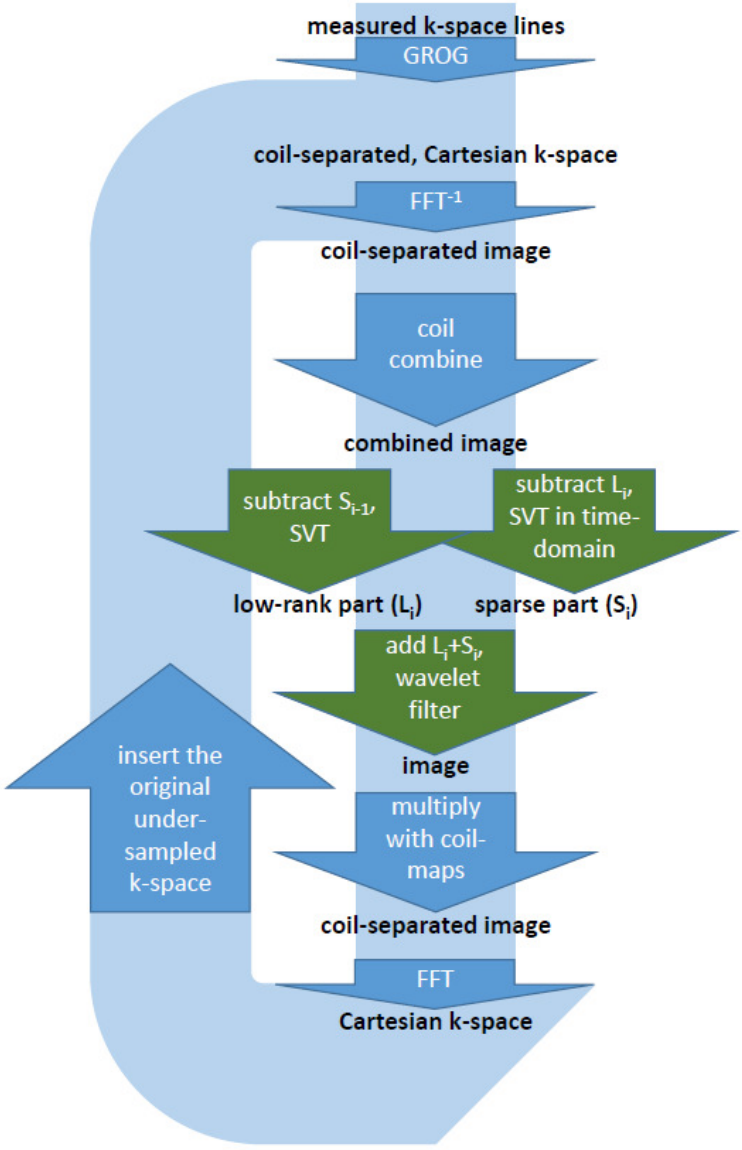

Figure 15: IR-CRISPI processing steps. Core of the algorithm (shown in green) is the separation into low-rank (L) and sparse (S) part. The index i shows the iteration number starting from 1, $S_0 = 0$.

fraction (EF), stroke volume (SV) and myocardial mass in diastole, a physician with 5 years of experience in cardiovascular imaging segmented the bSSFP reference images and IR-CRISPI cines. In doing so, the designated software cvi42 (Circle Cardiovascular Imaging Inc., Calgary, Canada) was used to segment the inner and outer contour of the left ventricle. Because sufficient magnetization is recovered before the second “R"-wave, synchronizing the 2D slices at the second systole and segmenting it together with the subsequent diastole was chosen to determine the functional parameters – applicable even for very slow pulses.

Two physicians contributed with their experience (5 years and 10 years in cardiovascular imaging, respectively) for the assessment of the myocardial viability of the patients. They independently determined appearance of LGE in the IR-CRISPI images and in the respective references. On a five point scale (0 meaning low, 1: rather low, 2: medium, 3: rather high and 4: high) following ratings were performed:

- transmurality (0: none, 1: 0–25%, 2: 25%–50%, 3: 50%–75%, 4: 75%–100%)
- the confidence in their LGE assessment (0: none, 1: unsure, 2: potential, 3: probable, 4: certain)
- overall image quality
- artifact level
- noise level
- image contrast between LGE and myocardium
- image contrast between LGE and blood

Additionally, it was recorded whether the physicians exploited the option to use multiple TI contrasts for the assessments based on IR-CRISPI. In the case of uncertain LGE existence, the ratings listed above were omitted.

Statistics For all numerical results described above a Bland-Altman analysis was performed. The Wilcoxon signed-rank test was determined to check for significance of the differences between IR-CRISPI and acquisitions of the corresponding breath-hold technique. The significance level was set to 0.05.

3.3 Setup

All measurements were done on a 3 T MR scanner (MAGNETOM Prisma$^{\text{fit}}$; Siemens Healthcare, Erlangen, Germany).

Reconstructions were performed using MATLAB (MathWorks, Natick MA, USA).

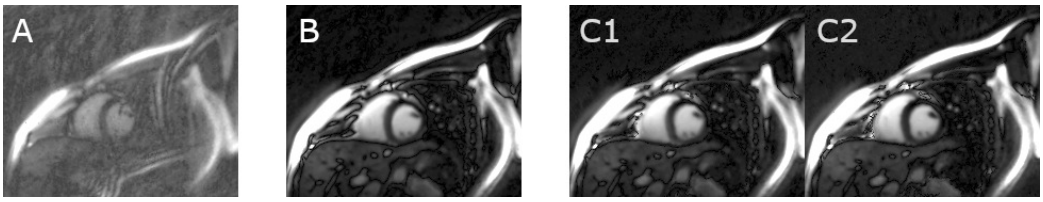

Figure 16: MOCO-MAP images of a healthy volunteer during nulled myocardium (TI: 713 ms). No contrast agent was applied in the volunteer study. Shown are the initial coil-combined image (A), the images using MOCO-MAP pseudo heartbeat reconstruction (B) and using MOCO-MAP reconstruction with iterative MOCO (C). The initial image (A) appears blurry with stripe-like undersampling artifacts. B and C1 are based on the full acquisition of 10.3 s, however, in contrast to the pseudo heartbeat concept, retrospectively cropping the data set at the 3.0 s-mark still allows for reconstruction with the iterative MOCO technique (C2).

4 Results

Imaging results using the methods MOCO-MAP and IR-CRISPI are presented in this section. MOCO-MAP was tested for feasibility and initial optimization of the measurement protocol, IR-CRISPI could be validated in a pre-clinical study.

4.1 MOCO-MAP

Both, MOCO-MAP implemented with iterative motion correction as well as with interpolated pseudo heartbeat (3.1.2) result in obvious improvement in terms of resolution and artifact removal with respect to basic gridding (see fig. 16). Using a binning of 10 spiral arms, which means a temporal resolution of 50–56 ms, visible improvement can be achieved in the first seven to nine iterations. In detail, the reconstruction with iterative motion correction allows to use a substantially smaller data set (fig. 16 C2). It generated results that were hardly distinguishable from the images based on the full data set (aside from being shorter in temporal direction). The shortening even resulted in a slightly reduced blurring in connection with patient motion.

The motion correction could be applied successfully. Decreased blurring due to cardiac motion can be shown in the results (fig. 17).

In figure 18 A a recorded ECG that did not properly capture all “R"-

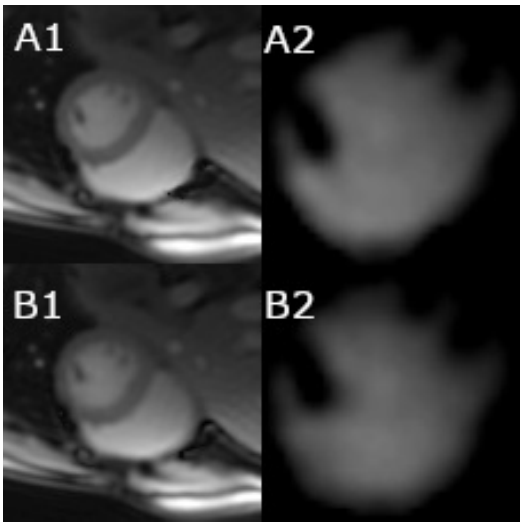

Figure 17: Images originating from the same acquisition shown in figure 16 at TI of 4.2 s. Compared are the images generated via MOCO-MAP reconstruction (A) and via MAP reconstruction (B) without motion correction. As the exponential fit corresponds to averaging while the diastole is significantly longer than the systole, leaving out the motion correction yields a blurry version of the image in diastole. To bring out blurring, the left ventricle is cut out in A2/B2. The blurring is visibly increased in the reconstruction without motion correction (B2).

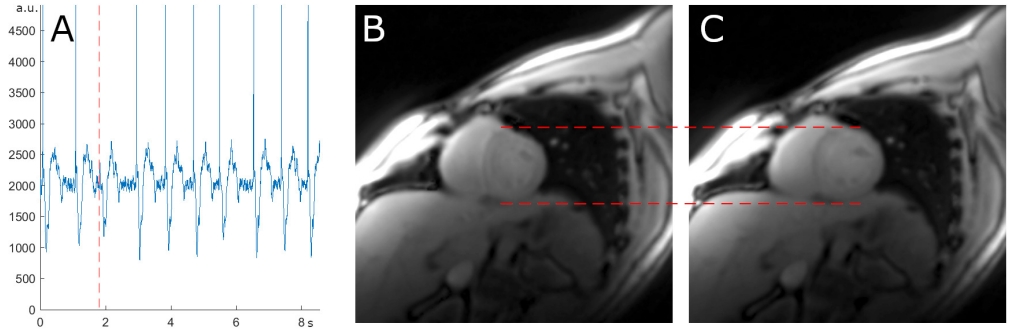

Figure 18: MOCO-MAP images from the same acquisition as shown in figure 16 at TI: 2.4 s and the ECG recording corresponding to that acquisition (A). They are reconstructed using iterative MOCO (B) and using pseudo heartbeat motion correction technique (C). Due to irregular pulse or bad signal recording of the ECG, the “R"-wave (maximum peaks, A) was not always correctly identified (missing wave is marked with red dashed line at ca. 2 s). The iterative MOCO reconstruction is independent from the ECG, consequently the systole is maintained in the result (B). The motion correction via the pseudo heartbeat reconstruction treats the systole at the same point in time as diastole (C).

waves is shown. Incorrect ECG recordings represent one possible error source introduced by the pseudo heartbeat reconstruction (also fig. 18). In this example the reconstruction took two heartbeats as one and interpolated the motion field accordingly. As a consequence, firstly, the motion here can not be corrected and secondly, the fit is based on wrong node points. This results in blurring in the myocardial region, comparable to, but usually in a less severe extent than, the blurring shown in figure 24.

Representing MOCO-MAP’s main feature, figure 19 illustrates the possibility to set TI retrospectively. Stepless setting of TI or depiction of the image series as one T_1 map (see figure 20) is possible, as the exponential relaxation parameters are already determined by curve fitting.

Figure 21 demonstrates the visibility of contrast agent induced delayed enhancement in the myocadium. Due to residual gadolinium concentration in connection with contrast agent enhanced imaging, characteristic inversion times like the TI of nulled myocardium are significantly lowered (compare results shown in 4.2).

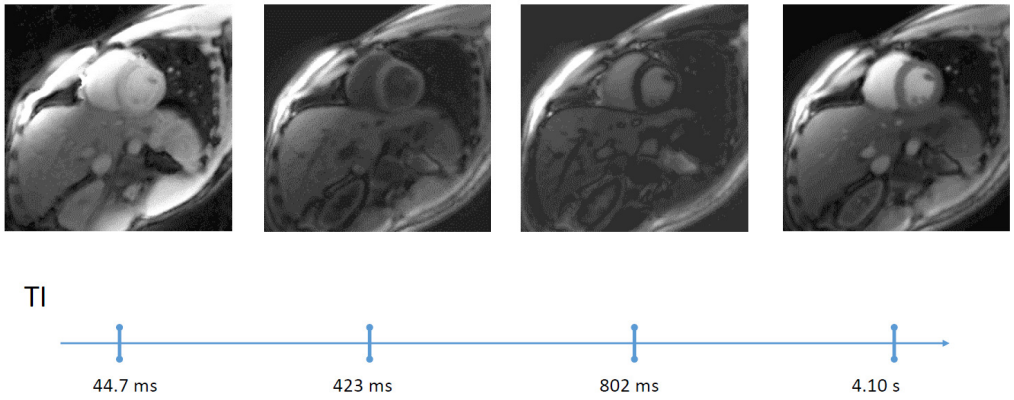

Figure 19: The MOCO-MAP reconstruction yields a time-resolved image series of the full signal recovery after an inversion preparation. Here the absolute signal intensities are shown. The result in standard LGE imaging is a static image at one fixed TI, the TIs of the depicted results are given in a timeline below.

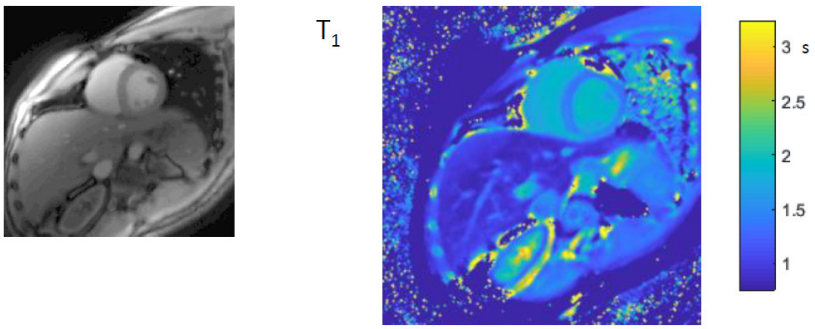

Figure 20: T_1 map (right) from the MOCO-MAP acquisition already shown multiple times (fig. 16 ff) and MOCO-MAP image at TI: 10.0 s shown for visual reference (left). The T_1 map was determined using the three pixel-wise fitting parameters M_0, M_∞ and T_1^* (see 2.3).

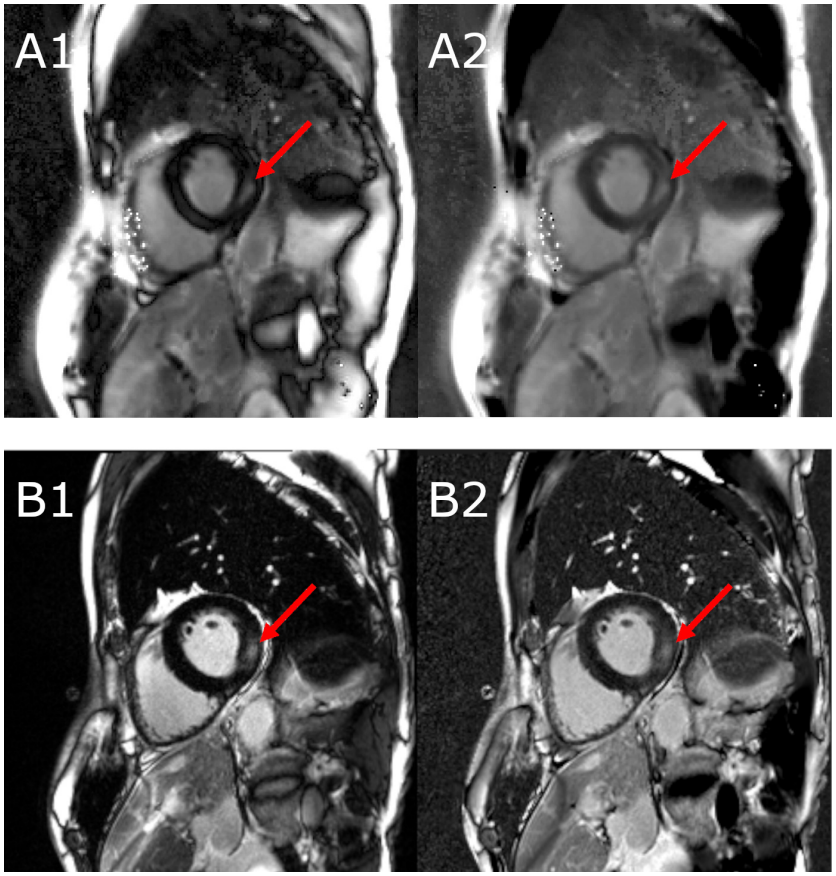

Figure 21: Delayed enhancement appearing in MOCO-MAP (A) and LGE reference images (B) of a patient with Fabry cardiomyopathy as part of the patient study. This MOCO-MAP result at TI: 335 ms as well as the images acquired with bSSFP reference technique both clearly show the bright spot in the lateral left ventricle (red arrow). A1 and B1 show the magnitude, whereas A2 and B2 are depicted in phase-sensitive representation. Single bright pixels at the border of the right ventricle are caused by erroneous phase-correction (A).

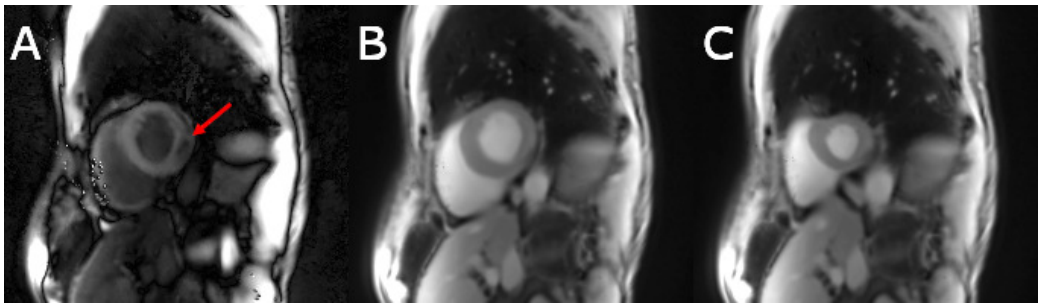

Figure 22: MOCO-MAP images at early TI (A: 235 ms) and late TI (B: 3.7 s, C: 4.1 s) from the same acquisition and patient as shown in figure 21. The detectability of altered T_1 because of contrast agent accumulation is not only given during zero-crossing of the myocardial signal (red arrow in A, compare with fig. 21). The cardiac cycle is resolved (B: diastole, C: systole).

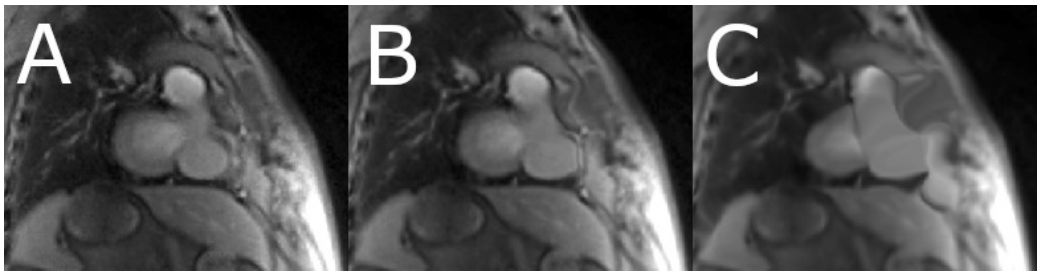

Figure 23: Example illustrating the error caused by motion correction. Here, a slice showing the basal myocardium (A) was motion corrected and warped back once (B) and five times (C). Instead of yielding the identical image, the moderate change after one application becomes severe after five.

In contrast to the static images from standard LGE imaging, MOCO-MAP images cover both, the relaxation process of the magnetization and the complete cardiac cycle (shown in figure 22).

Artifacts introduced by MOCO-MAP The following paragraph describes potentially appearing artifacts caused by iterative fitting and motion correction. While a single motion correction step often does not lead to obvious mis-registrations, repeated application of a determined vectorfield for motion compensation and subsequent reinstatement reveals inaccuracy of the method (see fig. 23). Incorporated in the iterative algorithm of MOCO-MAP this is one source of additionally introduced artifacts.

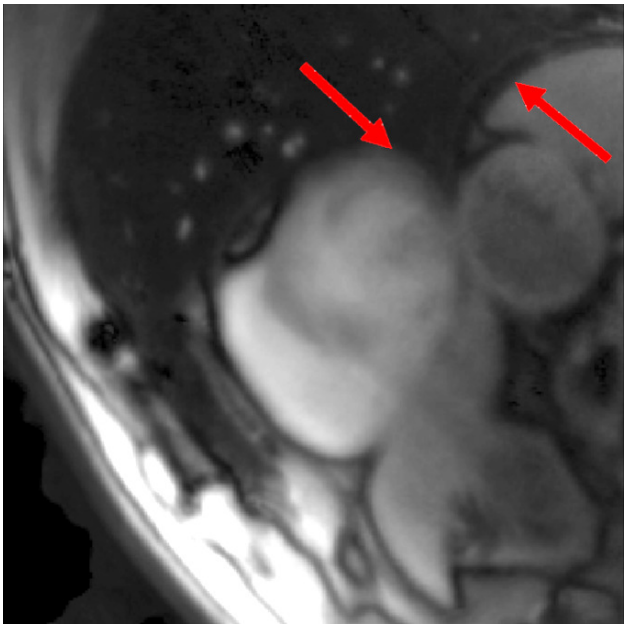

Figure 24: MOCO-MAP images from an acquisition of a thin slice (3 mm) at TI: 769 ms, which was part of the patient study. Weak signal to noise ratio because of the chosen slice thickness resulted in poor motion correction. Consequently, these inaccurate intensity shifts and smoothing by the pixel-wise fit lead to heavy blurring in the region of the the left ventricle (left arrow) and the papillary muscles. Edges of non-moving tissue are resolved well (compare the diaphragm in breath-hold, right arrow).

As a consequence of this inaccuracy, the exponential fit, which is supposed to enforce the physical model for identical tissue, will not only level out the intensity fluctuations due to undersampling, but also blur the edges of moving tissue (see fig. 24).

Additionally, for cases in which the intensity change due to residual motion exceeds the magnitude of the exponential signal development, least-squares fitting leads to unrealistic parameter determination (see fig. 25).

Finally, the quickly changing contrast at the beginning of the exponential signal relaxation leads to significant signal changes in a short period of time. Since the exponential fit is less accurate in this period of rapid change, mis-registrations can appear when using intensity based motion correction. For the reconstructed image this means gross distortions (see fig. 26).

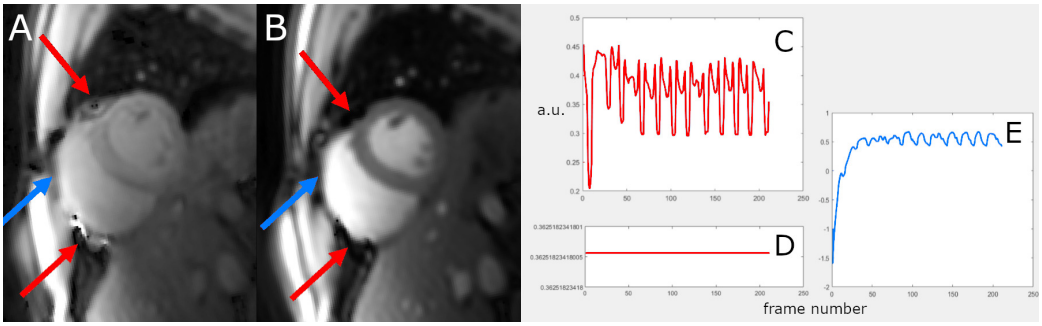

Figure 25: MOCO-MAP images of the same acquisition of the volunteer study shown in figures 16 ff represented by the exponentially fitted values at TI: 38 ms (A) and at TI: 11.8 s (B). The pixels marked with red arrows depict lung tissue and myocardium at different TIs, respectively. The signal yield of the two organs differs strongly, thus the signal course of pixels that contain both types of tissue over time can not be approximated as exponential curve (signal course C at the pixel location of the upper red arrow in A and B). If the motion correction is insufficient, the exponential fit results in crude averages or even just constant pixel intensities (i. e. $T_1^* = 0$, signal course D at the pixel location of the lower red arrow in A and B). The blue signal course (E) shows the signal of the MOCO-MAP result at the tip of the blue arrow for comparison. The exponential development here predominates signal change due to cardiac motion.

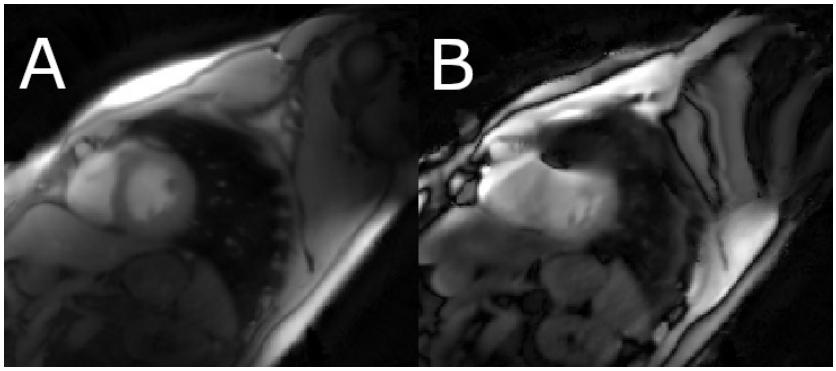

Figure 26: MOCO-MAP images acquired in the volunteer study at TI: 4.1 s (A) and at TI: 214 ms (B). Fast intensity change at this low TI (B) leads to mis-registrations due to the discrepancy between image series with fitted values and moving image.

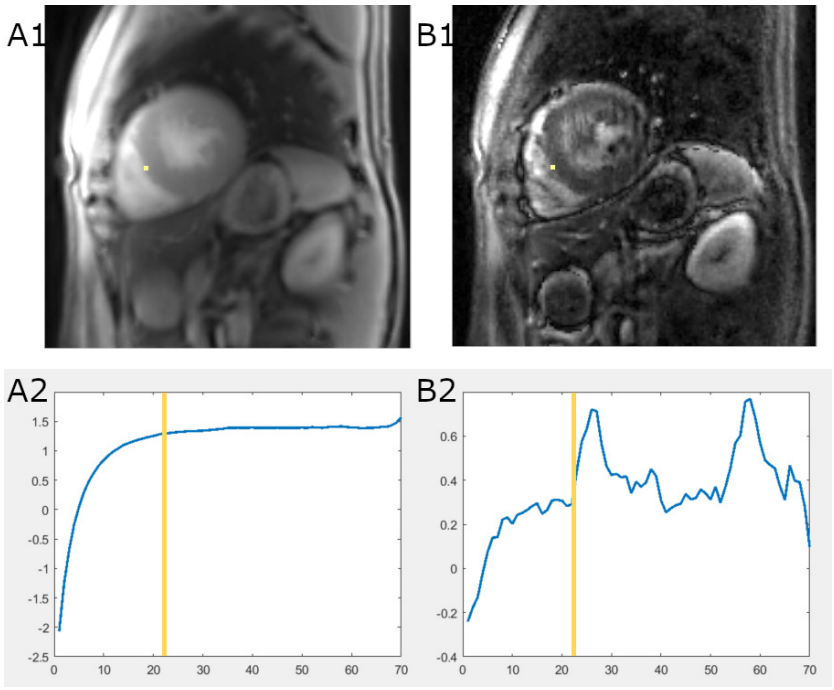

Figure 27: A1 and B1 show the IR-CRISPI image during reconstruction at 1.085 s after the inversion pulse. It is separated into low-rank (L) (A1 and A2) and sparse part (S) (B1 and B2). L represents the slowly changing background and thus is blurry in the myocardial area (A1). Quickly changing contributions are contained in S (B2). A2 and B2 show the phase-sensitive signal courses over time of the yellow marked pixel in A1 and B1, respectively. In A2 and B2 the acquisition time of L and S is marked with a yellow line, respectively.

4.2 IR-CRISPI

The results shown in figures 27 and 28 offer insight into the IR-CRISPI reconstruction principle. Figure 27 shows the low rank part, which is given by the singular value decomposition in combination with a soft threshold. This separate depiction confirms that the reconstruction is able to extract the image background in a way that maintains the overall signal course. The figure also shows the overlay of quickly changing signal in the part enforcing sparsity by soft threshold in the temporal domain. These are mainly regions with myocardial motion and with fast magnetization recovery. The reconstruction thus does not represent a strict separation into background and motion.

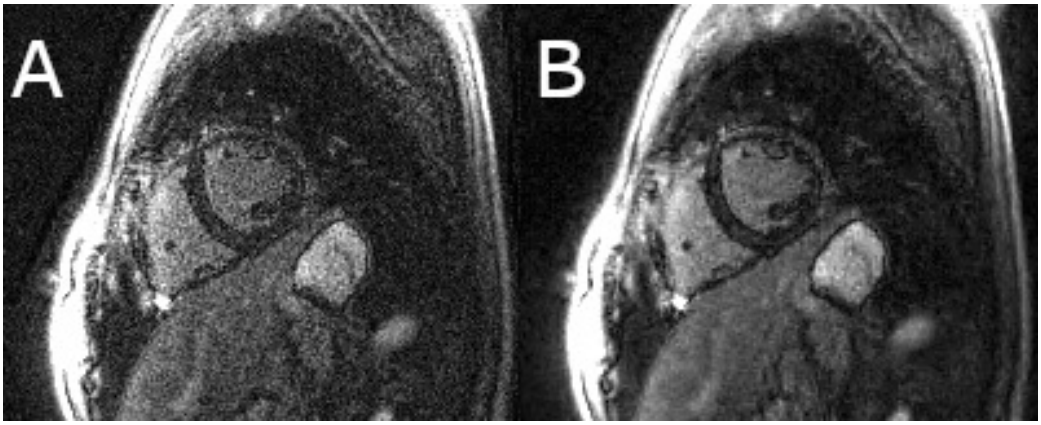

Figure 28: IR-CRISPI image at 335 ms shown without (A) and with applied wavelet constraint (B). Enforcing local smoothness in the spatial dimension by wavelet filtering is an effective tool to suppress noise. Near the zero-crossing of the signal (depicted here) this is easy to notice.

Figure 28 shows the additionally implemented denoising via wavelet filter. The low signal to noise ratio (SNR) during zero-crossing shows the importance of this step, which significantly improves recognition of physiological borders during the contrast of optimal LGE assessment.

An overview of the proposed IR-CRISPI imaging results from one measurement, which belong to one out of ten patients of the conducted study, is shown in figure 29. It comprises depiction of multiple slices, different inversion times, with the first second of the image series stored separately for the localization of late enhancement and the latter ≈ 2.5 s for the assessment of the myocardial function. As the reconstruction of the image series works with the complex data, retrospective representation as absolute valued as well as phase-sensitive (PSIR) image is possible. The total acquisition duration of the 15 slices took 105 s. Covering the whole left ventricle of the ten patients took 97 s on average.

4.2.1 Functional analysis

As IR-CRISPI is a real-time acquisition, the number of image frames per cardiac cycle varies. In contrast to the reference with 25 frames averaged from 12 cycles, one examined cycle in the patient study yielded 13 to 29

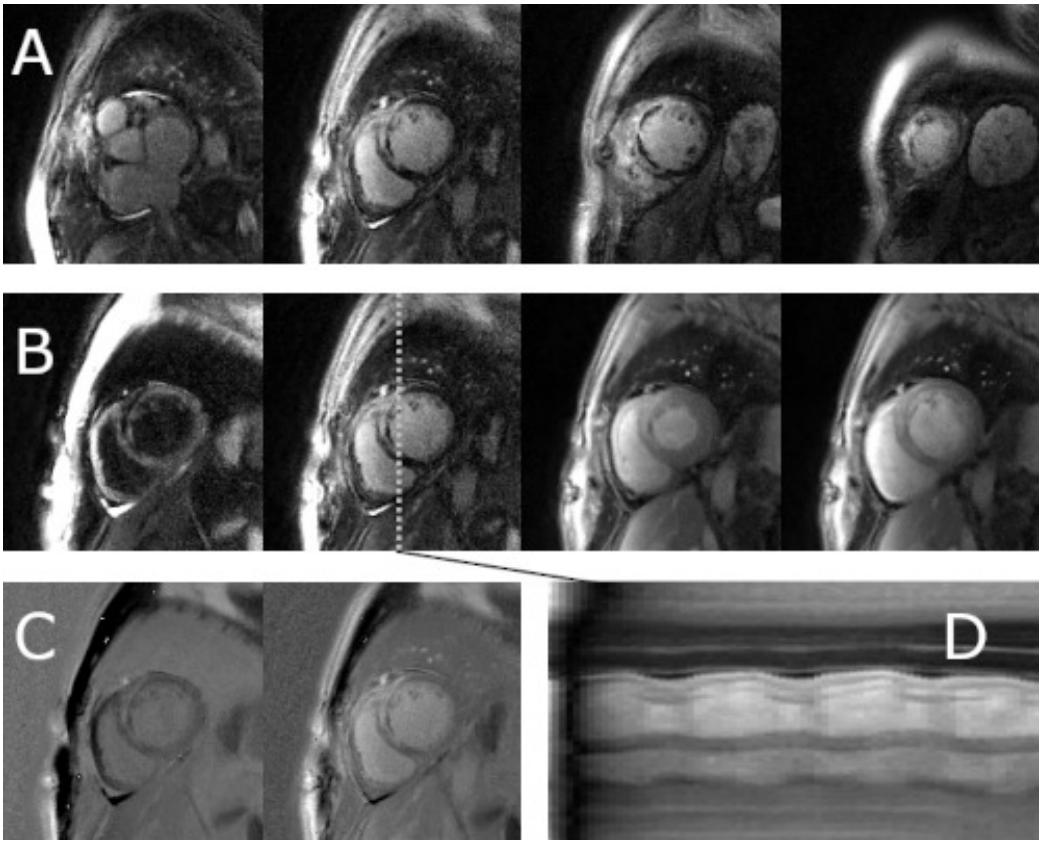

Figure 29: Overview of the results yielded by IR-CRISPI for one patient with acute antero-septal infarction and microvascular obstruction. Four of the total of fifteen acquired slices are shown in A (TI: 285 ms). The depicted myocardium exhibits a large enhancement stretching over the anterior and the antero-septal left ventricle (transmurality $> 75\,\%$). As the image series in B is absolute valued, the affected tissue first displays hypo-enhancement at TI: 185 ms (with the negative valued healthy myocardium shown bright) and then regular hyper-enhancement at TI: 285 ms (B, second from left). The phase-sensitive image series (C) shows zero valued pixels with an offset so they appear grey, here the enhancement is always bright in comparison to healthy myocardium. The image series also contains the dynamic information necessary to segment the myocardium for functional evaluation (B: third and forth image from left, TI: 985 ms and TI: 1385 ms). In D the signal course over time of the pixels indicated in B (second image from left), first, shows a rapid, almost full relaxation of the magnetization and three complete cardiac cycles afterwards. Previously published[39] under CC BY-NC 4.0 licence.

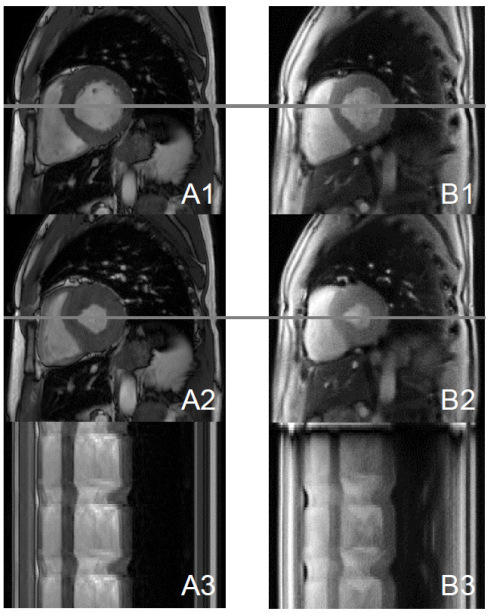

Figure 30: Comparison between breath-hold cine (A) and IR-CRISPI images (B) of a 49-year-old male patient with Fabry disease for diastole (1), systole (2) and the 1D signal course over time (3) from the pixels indicated with a grey line in the images above. The second cardiac cycle, which was used to segment the IR-CRISPI images for functional measures, can be approximated to be completely in steady-state like the reference images. Previously published[39] under CC BY-NC 4.0 licence.

reconstructed frames. The two different cines belonging to one patient are illustrated in figure 30. Manual volume segmentations could be performed for all patients included in the study, the functional parameters determined via IR-CRISPI alongside the evaluation from the breath-hold technique are plotted in figure 31.

The results are additionally compared with the reference by Bland-Altman-plots in figure 32. The biases from the functional evaluation together with the differences concerning the viability assessment are listed in table 1. The breath-hold technique compared with IR-CRISPI yields a 6.5 ml (3.8 %) larger EDV, 1.2 ml (1.7 %) smaller ESV, 2.3 % (4.8 %) larger EF, 7.7 ml (8.8 %) larger SV and 5.0 g (3.2 %) larger myocardial mass. The Wilcoxon signed-rank test shows that none of these discrepancies exceed the limit of signifi-

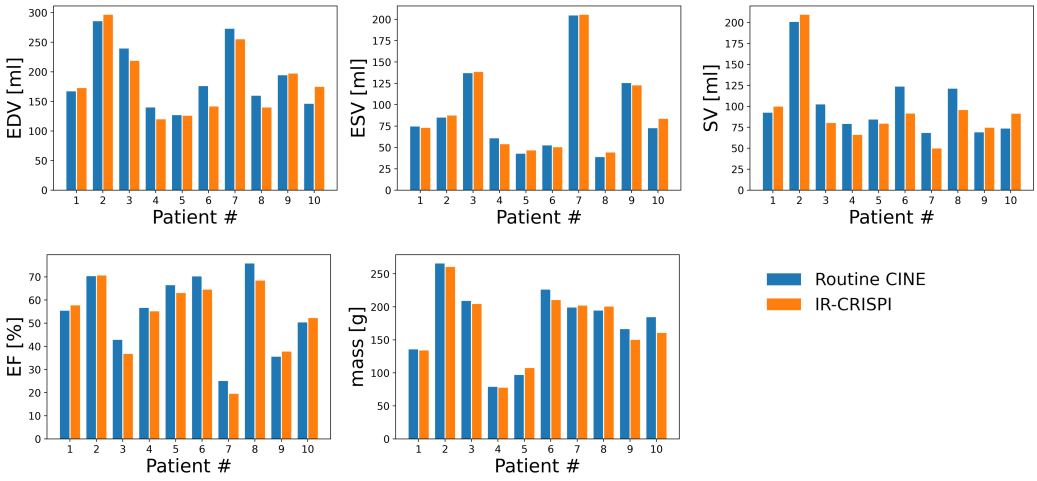

Figure 31: Results of the volume segmentations for all included patients. From the end-diastolic volume (EDV) and the end-systolic volume (ESV), stroke volume (SV), ejection fraction (EF) and the myocardial mass were determined.

cance (p-value regarding EDV: 0.38, ESV: 0.63, EF: 0.16, SV: 0.23, mass: 0.28).

	bias	confidence interval
EDV [ml]	6.54	35.5
ESV [ml]	-1.19	9.24
EF [%]	2.29	7.07
SV [ml]	7.72	31.5
mass [g]	4.96	20.2
transmurality	0.20	1.33
confidence in a.	0.05	1.31
overall quality	0.05	2.01
artifact level	0.75*	1.74
noise level	-0.8*	2.02
contrast LE/myoc.	0.47	1.73
contrast LE/blood	0.20	3.14

Table 1: Bias and confidence interval (1.96× standard deviation) of IR-CRISPI with respect to its reference breath-hold sequences. Significant differences are marked with an asterisk. Previously published[39] under CC BY-NC 4.0 licence.

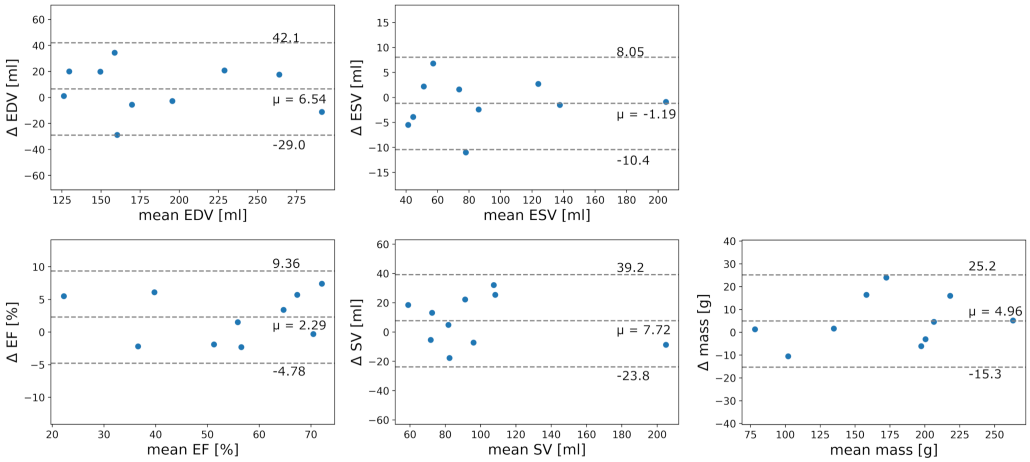

Figure 32: Bland-Altman-plots from IR-CRISPI vs. the respective breath-hold bSSFP acquisition. Shown are all 10 deviations between end-diastolic volumes (EDV), end-systolic volumes (ESV), ejection fractions (EF), stroke volumes (SV) and myocardial masses, with a confidence interval of 1.96 standard deviations. Previously published[39] under CC BY-NC 4.0 licence.

4.2.2 LGE imaging

An example of an LGE appearing on IR-CRISPI images is given in figure 33. The patient suffered from an acute infarction causing LGE, the transmurality of which was found to be larger than 75 % and it also involved the papillary muscles. While the routine exam yields a static image, via IR-CRISPI the signal development can be observed over time.

The ratings concerning the LGE assessment with IR-CRISPI and its reference bSSFP measurements are listed in table 2. The detection of LGE agreed for one reader for ten out of ten patients and for the other reader for nine out of ten patients between breath-hold sequence and IR-CRISPI. In detail, the thickness of the LGE, which is being assessed in the transmurality, in the ratings of the two readers differed at most by 25 %. The confidence the readers had in these assessments also differed by maximum one grade with respect to the other reader *and* with respect to the other acquisition method. Higher variance of the rating was observed for the perceived image contrasts, where the difference amounts up to 3 points on the given scale. The artifact and noise level assessments differed by up to 2 points between

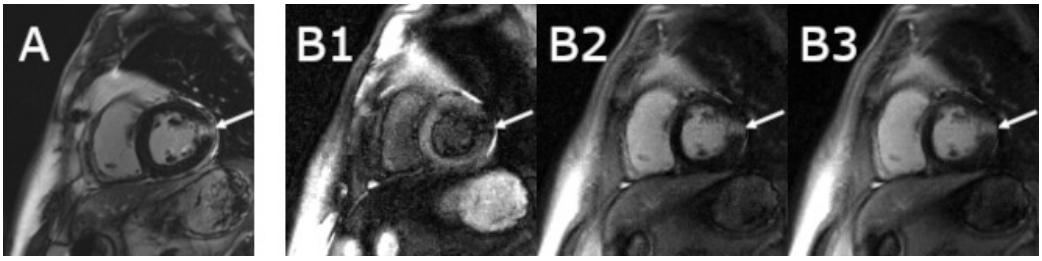

Figure 33: Comparison of LGE imaging via breath-hold bSSFP acquisition (A) and IR-CRISPI in magnitude depiction (B1-B3). The patient is a 54-year-old man with acute myocardial infarction in the infero-lateral mid-ventricular wall (white arrow) with involvement of the papillary muscles. For an early TI of 135 ms the infarcted tissue appears dark while healthy myocardium appears bright (B1), at and after the zero-crossing of the myocardial signal LGE appears bright (B2 TI: 235 ms, B3 TI: 260 ms). Previously published[39] under CC BY-NC 4.0 licence.

methods and raters, respectively.

The corresponding Bland-Altman evaluation can be read in the lower rows of table 1. The Wilcoxon signed rank test reveals that the biases between reference and IR-CRISPI are not significant except for the noise level, which is significantly lower (-0.80 points) for the breath-hold sequence, and for the artifact level, which is significantly higher (+0.75 points) with respect to it.

As the breath-hold acquisition yields static images, the readers could only view multiple TI-contrasts in the presented IR-CRISPI images. This feature was consistently used for all patients by both readers.

patient #	LGE present?		transmurality		confidence in assessment	
	reference	IR-CRISPI	reference	IR-CRISPI	reference	IR-CRISPI
1	no / no	no / no	0 / 0	0 / 0	3 / 3	4 / 3
2	yes / yes	yes / yes	4 / 4	4 / 4	4 / 4	4 / 4
3	yes / yes	yes / yes	3 / 3	3 / 3	3 / 4	4 / 3
4	no / no	no / no	0 / 0	0 / 0	4 / 4	4 / 4
5	yes / yes	**yes / no**	2 / 3	1 / 0	3 / **2**	**2** / 3
6	yes / yes	yes / yes	3 / 3	3 / 3	3 / 4	4 / 3
7	yes / yes	yes / yes	1 / 2	1 / 2	4 / 4	4 / 4
8	yes / yes	yes / yes	2 / 2	2 / 2	3 / 4	2 / 3
9	yes / yes	yes / yes	4 / 4	4 / 4	4 / 4	4 / 4
10	yes / yes	yes / yes	4 / 4	4 / 4	4 / 4	4 / 4
	multiple frames used?		artifact level		noise level	
1		yes / yes	0 / 1	0 / 1	0 / 0	2 / 1
2		yes / yes	3 / 1	1 / 1	1 / 0	2 / 2
3		yes / yes	3 / 2	1 / 1	4 / 2	2 / 2
4		yes / yes	2 / 1	0 / 0	1 / 0	1 / 1
5		yes / yes	2 / 2	1 / 1	1 / 1	2 / 1
6		yes / yes	2 / 2	0 / 1	2 / 2	2 / 1
7		yes / yes	1 / 2	1 / 1	1 / 1	2 / 2
8		yes / yes	0 / 1	1 / 1	0 / 1	2 / 2
9		yes / yes	2 / 2	0 / 2	1 / 1	2 / 2
10		yes / yes	0 / 1	0 / 1	0 / 0	2 / 2
	overall image quality		contrast LGE/myoc.		contrast LGE/blood	
1	3 / 4	3 / 3				
2	3 / 3	3 / 2	4 / 4	4 / 2	4 / 3	4 / 2
3	1 / 2	3 / 1	3 / 2	4 / 2	1 / 1	3 / 1
4	3 / 4	3 / 4				
5	2 / 2	3 / 3	3 / 2	2 /	1 / 2	2 /
6	2 / 2	4 / 2	3 / 2	4 / 1	1 / 1	4 / 1
7	4 / 3	4 / 2	4 / 3	4 / 2	3 / 3	3 / 0
8	3 / 3	3 / 2	2 / 3	2 / 1	3 / 2	3 / 1
9	2 / 3	3 / 2	4 / 4	4 / 3	4 / 4	4 / 2
10	4 / 4	4 / 2	4 / 4	4 / 3	3 / 4	4 / 1

rating from: (reader 1/reader 2);

transmurality of the LGE: (0: none, 1: 0-25 %, 2: 25-50 %, 3: 50-75 %, 4:75-100 %);

confidence in assessment: (0: none, 1: unsure, 2: potential, 3: probable, 4: certain);

other ratings: (0: low, 1: rather low, 2: medium, 3: rather high, 4: high)

Table 2: LGE ratings from two radiologists. Highlighted is the one case for which the readers disagreed with respect to LGE presence. Here, either reader had more confidence in the other acquisition technique, respectively. LGE/tissue contrast was not rated where no enhancement could be detected. In part published previously[39] under CC BY-NC 4.0 licence.

Additionally to the clearly defined LGE, patchy LGEs can appear. One

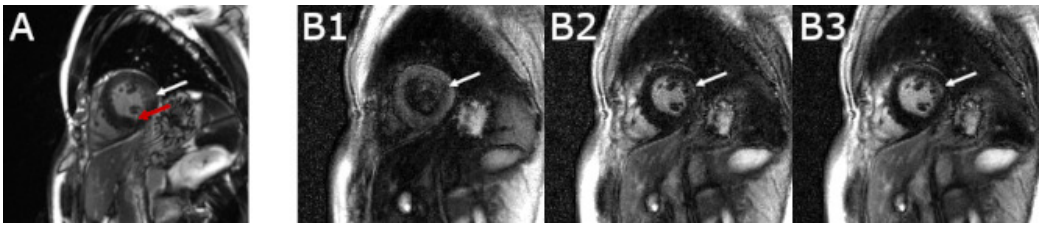

Figure 34: Focal patchy LGE of a 38-year-old male patient with Fabry cardiomyopathy (marked with a white arrow). While the enhancement does appear in the reference exam, an additional motion artifact is depicted (red arrow). IR-CRISPI constistently shows the LGE for the different image frames over time, here shown are TI: 235 ms (B1), 285 ms (B2), 310 ms (B3). Previously published[39] under CC BY-NC 4.0 licence.

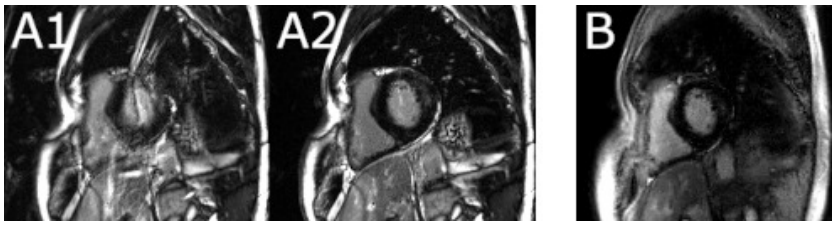

Figure 35: Heavy breathing artifacts (A1), they appeared as part of the same exam of the patient shown in figure 34. The artifacts render the acquisition non-diagnostic. The patient was able to repeat the breath-hold for this slice acquisition later, resulting in reduced artifact appearance (A2). IR-CRISPI was not affected by potential motion (B). Previously published[39] under CC BY-NC 4.0 licence.

example of this could be captured during the patient study. It is shown in figure 34.

Multiple patients of the study experienced difficulties to complete the breath-holds during the reference acquisitions. When dealing with patients with cardiac diseases, this a frequently encountered problem. If it is noticed by the examiner during the exam, the corresponding acquisition can be repeated. This is what happened in the case of the acquired reference shown in figure 35.

The occurrence of an enhancement just in the reference (example also listed in table 2, patient 5) can be seen in figure 36. A slice shift due to breathing motion can not be ruled out. However, directly adjacent slices do not show enhancements for IR-CRISPI either. Despite the breathing artifacts

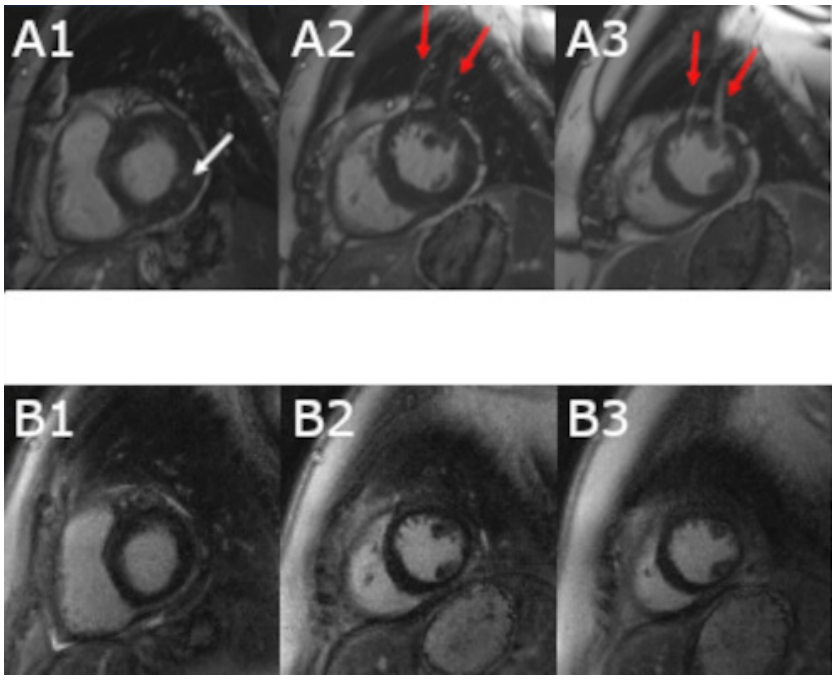

Figure 36: Three slices in optimal contrast for LGE depiction of a 66-year-old woman with Fabry cardiomyopathy, in the table 2 listed as #5. In A1 an enhancement can be seen in the image of the beath-hold technique (white arrow), while no anomaly can be observed via IR-CRISPI (B). Additional breathing artifacts of the reference method appear in A2 and A3. Previously published[39] under CC BY-NC 4.0 licence.

in the reference, which also appear bright, both readers labeled the shown dots as late gadolinium enhancement. Just the reader who was additionally asked to segment the left ventricle for functional evaluation observed a shallow enhancement in the lateral wall in the IR-CRISPI images series before one second after the acquisition start in the data rendered for cine evaluation.

5 Discussion

The implications that arise from the MOCO-MAP and IR-CRISPI results are discussed in the following section.

Generally, it can be inferred that a replacement of the segmented myocardial exam for a single-shot acquisition like MOCO-MAP or IR-CRISPI would come with significant time saving at the MR-scanner. To give exemplary values[‡], a standard exam comprising myocardial function and viability assessment of fourteen 8 mm slices takes up the time of

$$14 \cdot t_{cine} + 14 \cdot t_{LGE} + t_{TIscout} + 28 \cdot t_{gap}. \tag{30}$$

Assuming typical pauses to breath between the measurements (t_{gap}) of 10 s, this yields a minimally possible measurement time of

$$14 \cdot (9\,s + 11\,s) + 5\,s + 28 \cdot 10\,s = 9.4\,min. \tag{31}$$

With 2.5 s MOCO-MAP acquisitions, the total exam time could theoretically be reduced to 2.8 min ($14 \cdot 2.5\,s + 13 \cdot 10\,s$). Additionally, the patient comfort would increase due to breath-hold durations of just 2.5 s. Using IR-CRISPI this time can further be decreased to 1.5 min $(14 \cdot 6.5)$ s, as it is acquired in free breathing. ECG-triggering is disregarded in this calculation, but contributes twice the amount of trigger delays on the side of the standard exam. Similarly, the time regarding necessary settings at the scanner, e. g. adjustment of TI in the standard exam, also adds depending on the examiner to the duration of the standard exam.

5.1 MOCO-MAP

MOCO-MAP is motivated by a great potential for acceleration and a versatile myocardial exam. Although the realization is possible to some extent, until now motion could never be captured accurately. Artifacts can be

[‡]The durations derive from the MR measurement parameters described in sub-sections 3.1.4 and 3.2.3.

misinterpreted as LGE and insufficient exponential fits can lead to flaws in the calculation of T_1. A slice-by-slice MOCO-MAP acquisition could yield the information necessary for the left-ventricular function evaluation and T_1 mapping or the function plus viability evaluation when featuring contrast agent application.

Although the MAP-algorithm exhibits great robustness regarding undersampled data reconstruction,[47] repeated motion correction cancels to some extent the benefit of the model-based approach. Image registration is intrinsically already an error afflicted operation, because continuous motion of continuous matter is projected on discrete pixel locations. However, for iterative methods like MOCO-MAP this happens in an accumulating manner. Non-rigid motion correction and algorithms incorporating it are also prone to be erroneous or inaccurate, when the regularization parameters are not adjusted for the specific case. Additionally, the signal characteristics of undersampled IR data are not well suited for image registration. Reasons for this comprise the fact that most registrations algorithms are based on signal intensity matching,[23] while the inversion leads to constantly changing intensity. Even small differences in image contrast between moving and fixed input images, e. g. introduced by the exponential fit, causes detection of motion where there is none. The other reason is that registration algorithms are more accurate for well resolved edges. This conflicts with the iterative algorithm, which is initialized with a blurry image.

A dependency on the used k-space trajectory and its corresponding undersampling artifact pattern was observed. The underlying effect is that these intensity fluctuations are misinterpreted as motion. This effect, however, is for the most part eliminated by median filtering the motion field in time direction.

Finally, conventional image registration algorithms are time-consuming and easily take up more than two-thirds of the reconstruction time. Thinkable as a solution is a tensor or artificial intelligence based approach for motion correction, which would have to be designed to satisfy the special conditions for IR image data registration.

Motion correction, however, is still a powerful tool in cardiovascular MR.

The concept of combining, for example, single instead of iterative motion correction with the application of a physical model can lead to superior quality of images reconstructed from undersampled data with less signal loss in the walls of the right and left ventricle.[2] One of the main problems of cardiovascular imaging with patients affected in that region is the difficulty for them to hold their breath. In regions of interest where breathing motion can be approximated as rigid transformation rigid correction of respiratory motion represents another field for acceleration of myocardial imaging in free breathing.[15] Also noteworthy is the fact that in a 2D acquisition not all components of the motion is captured as deformation of flexible tissue. While in-plane motion can theoretically be corrected, through-plane motion represents a significant challenge in cardiac 2D imaging. One option to overcome this problem is to expand the acquisition protocol to 3D.[2] This strategy, however, comes with the difficulty of distinctly decreased sampling per time interval, meaning additional undersampling.

5.2 IR-CRISPI

A solution to surpass the problems faced using MOCO-MAP and, additionally, to advance to a free-breathing method was discovered. An algorithm designed for the reconstruction of undersampled cine data was transferred and tested on the data, previously acquired for MOCO-MAP. This approach was improved, surveyed and published. It will be presented in this section.

IR-CRISPI[39] combines functional and late gadolinium enhancement imaging using one magnetization inversion per acquired slice. It has been validated in a small patient study of 10 patients evaluated by two physicians. The mean acquisition time for the whole left ventricle could be kept below 100 s on average, while the quality was not rated significantly different from the distinctly longer standard exams. Additionally, IR-CRISPI works without breath-holds, while the standard exam requires breath-holds, at least the number of acquired slices times two. Problems often faced in CMR exams include the inability of patients to hold their breath or even stay awake. Here, IR-CRISPI is a valid solution, which is not dependent on the ability

of the patient to execute breathing commands. Artifacts originating from the reconstruction algorithm could largely be eliminated to an extent that the LGE images reached lower artifact levels than the presented reference exam (average rated level of 0.75 instead of 1.5 for the reference). As the low-rank plus sparse approach is able to exploit the redundancy of dynamic image data, while maintaining the motion, advantages can be seen especially with respect to motion correction approaches featuring image registration. Image distortion, blurring and consequential artifacts can be avoided, image reconstruction time can be reduced significantly (MOCO-MAP about 12 h vs. IR-CRISPI about 0.5 h per reconstructed slice).

The choice of real-time[36] imaging protocols instead of segmented acquisitions has already been recommended for cardiac cine and LGE assessments in the context of patients affected with arrhythmia or dyspnoea.[28] Reason for this is the obvious benefit of a prevention of motion artifacts. IR-CRISPI additionally offers the practical aspect of the combined measurement for cine and LGE imaging without the need for additional TI-scout sequence runs. This comes with the benefit of automatically measuring at consistent slice positions during cine and LGE acquisitions. Two separate measurements bring the risk of losing the imaging reference position due to patient body motion. They are often more than 15 minutes apart, because the contrast agent is usually applied between the measurements.[26] The combination of the sequences into one is also time-efficient, because the applied non-selective inversion pulses need to have time gaps for magnetization recovery. These gaps can partially be used to acquire the data needed for cine reconstruction, as the latter part of the exponential curve is narrow and the residual contrast change does not hamper manual volume segmentation for functional evaluation. This means that the total LGE plus cine acquisition time is inherently shorter than the separate sequential measurements. This also means just one completion of the iterations is needed for the image reconstruction. As sampling periods steadily become shorter, the additional information from a combined reconstruction can facilitate the determination of the low-rank part.

After the preceding validation of functional evaluation via real-time imag-

ing using spiral sampling (CRISPI[13]), one goal of this research was to replicate these promising results. As no significant differences between the functional parameters via breath-hold technique and IR-CRISPI could be detected, this goal was achieved. However, standard deviations of the difference between both methods for EDV and SV were found to be higher in the presented study. This is not necessarily caused by the difficulty to segment data originating from an MR sequence with magnetization preparation. Instead, the reason might also lie in the selection of subjects in the study. In contrast to the CRISPI study, in which 78 % subjects have been healthy participants[13] and all of them were able to perform the requested breath-holds, IR-CRISPI was applied in a pure patient study. Subjects with difficulties to hold their breath and with irregular pulses have been included in the study. The according consequences for imaging have been demonstrated (e. g. in fig. 35). These conditions may not only cause motion artifacts, but predictably lead to deviations in the segmented volumes, as the parameters via the real-time method are inherently subject to these fluctuations. To mention the order of magnitude of normal deviations, 3.9 % to 10.2 % of interobserver variability[31] even for data exclusively originating from segmented cine acquisitions have been reported.

When comparing LGE representations of the reference with IR-CRISPI, it is important to keep in mind that IR-CRISPI was acquired 8-9 minutes after contrast agent application to keep the acquisition time with optimal contrast for LGE assessment (later than 10 minutes after application) for the medically approved sequences.[26] Hypothetically this could be the reason of the deviation regarding a small LGE appearing just in the images acquired via breath-hold technique (fig. 36). Other explanations could be small differences in the cardiac phase or small slice gaps occurring due to the acquisition in different breathing states in IR-CRISPI images. Inter-reader variation of the contrast ratings regarding IR-CRISPI was found to be high with mean differences of 1.71 between LGE and myocardium and 2.43 between LGE and blood (reference: 0.63 LGE/myoc. and 0.50 LGE/blood). Apart from the different imaging characteristics due to choice of MR-sequence, one aspect leading to this could be the option to view multiple TI-contrasts per patient

and slice, which was exploited explicitly. As physicians are typically not supplied with this option and dynamic results offer more depth to review the data, deviations in handling the TI-contrast setting are to be expected. Furthermore, a learning effect could improve long-term performance of working with IR-CRISPI. The dynamic fashion of the IR-CRISPI's LGE representation as stack of consecutive images also turned out to be advantageous by indicating if a depicted anomaly represents a residual artifact or an actual medical finding by either consistent or random anomaly appearance. In general, the shortened acquisition time and IR-CRISPI's implementation as spoiled gradient echo mean a decrease in SNR compared with the standard bSSFP acquisitions.[33,38]

Despite these observed deviations, benefits and disadvantages between the two LGE acquisition techniques seem to complement one another, as the mean quality rating for IR-CRISPI is 2.80 and for the breath-hold technique it is 2.85. Furthermore, both readers independently determined the transmuralities to be equal for the two techniques regarding the nine patients, for whom they agreed on LGE existence. Within the limits of the conducted study, this strongly indicates that both presented LGE imaging techniques lead to assessments of equivalently severe tissue affectation. Additionally, the difference in the ratings *between* the two readers amounted to only one out of five scale points, which suggests a small inter-reader disagreement for that matter. This is also reflected in the similar confidence the readers had regarding their assessment using the respective technique (average of 3.55 for IR-CRISPI and 3.60 for the breath-hold technique). Based on this consistency, moving towards clinical studies, which allow statistically meaningful statements, stands to reason. Not included in the study, but also present, are patients completely unable to hold their breath. While a medical MR exam in this setting was rescheduled or not possible at all, IR-CRISPI could have served as an adequate alternative for these patients.

Development in the field of MR imaging causes the gap of spatial and temporal resolutions between segmented and real-time techniques to become smaller or even to vanish.[51,57] Other current research already proposes real-time acquisition for LGE assessment.[55] The combination of magnetization

recovery with cine imaging is also an idea that was realized previously.[2,19] Related research was able to improve basic compressed sensing by incorporating motion correction into the reconstruction algorithm. This represents a mix of the core elements used in the MOCO-MAP and the IR-CRISPI reconstructions.[49] Regarding sampling schemes, the step towards non-continuous sampling in form of a sampling scheme called sparse sampling could be performed. This benefits the reconstruction using separation into low-rank and sparse part, similar to this work, leading to high spatial and temporal resolution.[8] Unique in IR-CRISPI is the combined measurement for functional and LGE assessment using low-rank plus sparse reconstruction and spiral acquisition. This enables better coverage of the outer k-space, while no post-correction is needed because of the application of the GSTF-based pre-emphasis (1.3.5). IR-CRISPI's echo time of 0.84 ms additionally helps to reduce effects caused by the relaxation T_2^*.

Through-plane motion is a subject which still has to be addressed in future studies. To deal with possible errors in volume segmentations or missing details because of a slice shift, either negligibility of respiratory though-plane motion has to be proven or corrections like respiratory gating[24] or techniques that take the third dimension into account[16] have to be integrated into the IR-CRISPI measurement protocol.

To give a prospect, the advantages of IR-CRISPI might suggest a broader medical indication for the cardiac exam other than just for patients with difficulties to hold their breath. Significant exam time savings have an economic impact and promote the use of real-time protocols like IR-CRISPI, provided that the quality can be maintained. Future studies might also consider the option of imaging contrast agent wash in and wash out dynamics via IR-CRISPI, as this becomes more accessible for the CMR standard exam due to the shortened time increment between measurements. It might allow to explore a source of new diagnostic information.[56]

6 Conclusion

The method of MOCO-MAP could successfully be implemented, and its feasibility was shown. Compared with Cartesian MR measurement protocols, it exhibits high sampling efficiency. However, a susceptibility to reconstruction flaws was shown. The likelihood of introducing errors via image registration is considerably increased when applied in iterative algorithms as well as for image series with constantly changing image contrast.

IR-CRISPI, however, resembles a way of learning from the challenges occurring in MOCO-MAP. Via IR-CRISPI an acceleration of the cardiovascular MR exam in the order of magnitude of 10-fold can be achieved, potential diagnostic information can be gained if used in addition to the standard exam for any patient. If the patient experiences problems to hold his or her breath, results acquired via IR-CRISPI are likely to reach higher quality than via conventional exam. The presented results in this work are not only promising, but already turned out to deliver a second source of information to support the results of the standard exam for the patients that agreed to take part in the IR-CRISPI study. Access to the IR-CRISPI images was proactively requested by the examining physicist, when the finding appeared to be ambiguous.

In this work, the potential and difficulties of new MR acquisition protocols have been shown. The need for improvement in the field of LGE imaging should be recognized, too. Although IR-CRISPI and the standard exam presented as reference have their distinct advantages, medical findings originating by just one of these methods should not be seen as an absolutely secure foundation for a diagnosis. With their ratings regarding LGE images described in 4.2.2, the physicians revealed that neither IR-CRISPI (mean rated image quality of 2.80) nor the actually practiced standard exam (rated with 2.85) delivers results that reach the limit of being “rather high" quality (3.0), which means they are far from being high quality (score of 4.0). Until a satisfactory standard using a single CMR imaging technique will be established, using both, real-time techniques and segmented acquisition, or inclusion of another exam modality, have to be considered.

This work aims to share aspects of how to enhance diagnostic value in cardiovascular MR. At this point there should be no doubt that further development of IR-CRISPI or similar MR measurement protocols and their introduction to the daily medical routine would mean a step forward in the field of radiology.

7 Summary

This work deals with the acceleration of cardiovascular MRI for the assessment of functional information in steady-state contrast and for viability assessment during the inversion recovery of the magnetization. Two approaches are introduced and discussed in detail. MOCO-MAP uses an exponential model to recover dynamic image data, IR-CRISPI, with its low-rank plus sparse reconstruction, is related to compressed sensing.

MOCO-MAP is a successor to model-based acceleration of parameter-mapping (MAP) for the application in the myocardial region. To this end, it was augmented with a motion correction (MOCO) step to allow exponential fitting the signal of a still object in temporal direction. Iteratively, this introduction of prior physical knowledge together with the enforcement of consistency with the measured data can be used to reconstruct an image series from distinctly shorter sampling time than the standard exam ($< 3\,\mathrm{s}$ opposed to about $10\,\mathrm{s}$). Results show feasibility of the method as well as detectability of delayed enhancement in the myocardium, but also significant discrepancies when imaging cardiac function and artifacts caused already by minor inaccuracy of the motion correction.

IR-CRISPI was developed from CRISPI, which is a real-time protocol specifically designed for functional evaluation of image data in steady-state contrast. With a reconstruction based on the separate calculation of low-rank and sparse part, it employs a softer constraint than the strict exponential model, which was possible due to sufficient temporal sampling density via spiral acquisition. The low-rank plus sparse reconstruction is fit for the use on dynamic and on inversion recovery data. Thus, motion correction is rendered unnecessary with it.

IR-CRISPI was equipped with noise suppression via spatial wavelet filtering. A study comprising 10 patients with cardiac disease show medical applicability. A comparison with performed traditional reference exams offer insight into diagnostic benefits. Especially regarding patients with difficulty to hold their breath, the real-time manner of the IR-CRISPI acquisition provides a valuable alternative and an increase in robustness.

In conclusion, especially with IR-CRISPI in free breathing, a major acceleration of the cardiovascular MR exam could be realized. In an acquisition of less than 100 s, it not only includes the information of two traditional protocols (cine and LGE), which take up more than 9.6 min, but also allows adjustment of TI in retrospect and yields lower artifact level with similar image quality.

8 Zusammenfassung

Diese Arbeit behandelt die Beschleunigung der kardiovaskulären MRT zum Erfassen funktioneller Information bei Steady-State-Kontrast und zur Untersuchung der Vitalität bei Wiederherstellung der Magnetisierung nach ihrer Inversion. Zwei Ansätze werden eingeführt und im Detail diskutiert: MOCO-MAP, welches ein exponentielles Modell nutzt, um dynamische Daten zu rekonstruieren, und IR-CRISPI, welches mit seinem “low-rank plus sparse"-Algorithmus mit Compressed Sensing verwandt ist.

MOCO-MAP ist der Nachfolger der modellbasierten Beschleunigung des Parameter-Mappings (MAP) für die Anwendung im Bereich des Myokards. Hierzu wurde es mit einer Bewegungskorrektur (MOCO) versehen, um exponentielles Fitten eines unbewegten Objects in Zeitrichtung zu ermöglichen. Das Einbringen dieses physikalischen Vorwissens zusammen mit dem Erzwingen von Konsistenz mit den Messdaten wird dazu genutzt, iterativ eine Bildfolge aus Daten einer deutlich kürzeren Messung als herkömmlich zu rekonstruieren (< 3 s gegenüber ca. 10 s). Die Ergebnisse zeigen die Umsetzbarkeit der Methode sowie die Nachweisbarkeit von Delayed Enhancements im Myokard, aber deutliche funktionelle Abweichungen und Artefakte bereits aufgrund von kleinen Ungenauigkeiten der Bewegungskorrektur.

IR-CRISPI geht aus CRISPI hervor, welches zur Auswertung von funktionellen Echtzeitdaten bei konstantem Kontrast dient. Mit der Rekonstruktion durch getrennte Berechnung von niedrigrangigem und dünnbesetztem Matrixanteil wird hier bei der Datenrekonstruktion weniger stark eingeschränkt als bei einem strikten exponentiellen Modell. Die spirale Aufnahmeweise erlaubt hierzu ausreichend effiziente k-Raumabdeckung. Die

“low-rank plus sparse"-Rekonstruktion ist kompatibel mit dynamischen und mit Inversion-Recovery-Daten. Eine Bewegungskorrektur ist folglich nicht nötig.

IR-CRISPI wurde mit einer Rauschunterdrückung durch räumliche Wavelet-Filterung versehen. Eine Studie, die 10 Patienten einschließt, zeigt die Eignung für die medizinische Anwendung. Der Vergleich mit herkömmlichen Aufnahmetechniken lässt auf den gewonnenen diagnostischen Nutzen schließen. Besonders für Patienten, die Schwierigkeiten mit dem Luftanhalten haben, eröffnet diese Echtzeitaufnahmemethode eine wertvolle Alternative und erhöhte Stabilität.

Am Ende konnte gerade mittels IR-CRISPI eine bemerkenswerte Beschleunigung der kardiovaskulären MR-Untersuchung verwirklicht werden. Trotz der kurzen Aufnahmezeit von weniger als 100 s für den kompletten linken Ventrikel schließt es nicht nur die Information zweier herkömmlicher Protokolle mit ein (Cine und LGE), die zusammen mehr als 9,6 min dauern, sondern es erlaubt zusätzlich auch das Einstellen der TI-Zeit im Nachhinein und liefert Ergebnisse mit geringerem Artefaktlevel bei ähnlicher Bildqualität.

References

1. Balakrishnan G, Zhao A, Sabuncu MR, Guttag J, Dalca AV. VoxelMorph: A Learning Framework for Deformable Medical Image Registraion. *IEEE Trans Med Imaging.* 2019;38(8):1788–1800

2. Becker KM, Blaszczyk E, Funk S, Nuesslein A, Schulz-Menger J, Schaeffter T, Kolbitsch C. Fast myocardial T_1 mapping using cardiac motion correction. *Magn Reson Med.* 2019;00:1–14

3. Beer M, Stamm H, Machann W, Weng A, Goltz JP, Breunig F, Weidemann F, Hahn D, Köstler H. Free breathing cardiac real-time cine MR without ECG triggering. *Int J Cardiol.* 2010;145(2):380–382

4. Brown RW, Cheng YN, Haacke EM, Thompson MR, Venkatesan R. MAGNETIC RESONANCE IMAGING – Physical Principles and Sequence Design, second edition. *Wiley-Liss* 2014;ISBN 978-0-471-72085-0

5. Candès EJ, Romberg J, Tao T. Robust uncertainty principles: exact signal reconstruction from highly incomplete frequency information. *IEEE Trans Inf Theory.* 2006;52(2):489–509

6. Caravan P, Farrar CT, Frullano L, Uppal R. Influence of molecular parameters and increasing magnetic field strength on relaxivity of gadolinium- and manganese-based T1 contrast agents. *Contrast Media Mol Imaging.* 2009;4(2):89–100

7. Carr JC, Simonetti O, Bundy J, Li D, Pereles S, Finn JP. Cine MR Angiography of the Heart with Segmented True Fast Imaging with Steady-State Precession. *Radiology.* 2001;219:828–34

8. Christodoulou AG, Zhang H, Zhao B, Hitchens TK, Ho C, Liang Zhi-Pei. High-Resolution Cardiovascular MRI by Integrating Parallel Imaging With Low-Rank and Sparse Modeling. *IEEE Trans Biomed Eng.* 2013;60(11):3083–91

9. Curtis AD, Cheng HM. Primer and Historical Review on Rapid Cardiac CINE MRI. *J Magn Reson Imaging.* 2020;55(2):373–388

10. Davids M, Ruttorf M, Zöllner FG, Schad LR. Fast and Robust Design of Time-Optimal k-Space Trajectories in MRI. *IEEE Trans Med Imaging.* 2015;34(2):564–77

11. Deichmann R, Haase A. Quantification of T_1 Values by SNAPSHOT-FLASH NMR Imaging. *J Magn Reson.* 1992;96:608–12

12. Donoho D. Compressed sensing. *IEEE Trans Inf Theory.* 2006;52(4):1289–1306

13. Eirich P, Wech T, Heidenreich JF et al. Cardiac real-time MRI using a pre-emphasized spiral acquisition based on the gradient system transfer function. *Magn Reson Med.* 2020;00:1-–14

14. Elster AD. Courtesy of Allen D. Elster, `MRIquestions.com`

15. Feng L, Benkert T, Block KT, Sodickson DK, Otazo R, Chandarana H. Compressed Sensing for Body MRI. *J Magn Reson Imaging.* 2017;45(4):966–87

16. Feng L, Coppo S, Piccini D, Yerly J, Lim RP, Masci PG, Stuber M, Sodickson DK, Otazo R. Five-Dimensional Whole-Heart Sparse MRI. *Magn Reson Med.* 2018;79(2):826–38

17. Fieno DS, Kim RJ, Chen EL, Lomasney JW, Klocke FJ, Judd RM. Contrast-enhanced magnetic resonance imaging of myocardium at risk: distinction between reversible and irreversible injury throughout infarct healing. *J Am Coll Cardiol.* 2000; 36:1985–91

18. Hamilton JI, Franson D, Seiberlich N. Recent Advances in Parallel Imaging for MRI. *Prog Nucl Magn Reson Spectrosc.* 2017;101:71–95

19. Hamilton JI, Jiang Y, Eck B, Griswold M, Seiberlich N. Cardiac cine magnetic resonance fingerprinting for combined ejection fraction, T1 and T2 quantification. *NMR Biomed.* 2020;33(8):e4323

20. Hunold P, Schlosser T, Vogt FM et al. Myocardial late enhancement in contrast-enhanced cardiac MRI: distinction between infarction scar and non-infarction-related disease. *Am J Roentgenol.* 2005;184:1420–6

21. Jackson IJ, Meyer CH, Nishimura DG, Macovski A. Selection of a Convolution Function for Fourier Inversion Using Gridding. *IEEE Trans Med Imaging.* 1991;10(3):473–8

22. Jehenson P, Westphal M, Schuff N. Analytical method for the compensation of eddy-current effects induced by pulsed magnetic field gradients in NMR systems. *J Magn Reson 1969.* 1990;90:264–278.

23. Jenkinson M. Image Registration and Motion Correction. *Centre for Functional MRI of the Brain (FMRIB), University of Oxford*

24. Kellman P, Larson AC, Hsu LY, Chung YC, Simonetti OP, McVeigh ER, Arai AE. Motion-Corrected Free-Breathing Delayed Enhancement Imaging of Myocardial Infarction. *Magn Reson Med.* 2005;53:194–200

25. Kellman P, Arai AE. Cardiac Imaging Techniques for Physicians: Late Enhancement. *J Magn Reson Imaging.* 2012;36:529–542

26. Kim RJ, Shah DJ, Judd RM. How We Perform Delayed Enhancement Imaging. *J Cardiovasc Magn Reson.* 2003; 5:613–35

27. Klein S, Staring M, Murphy K, Viergever MA, Pluim JPW. elastix: A Toolbox for Intensity-Based Medical Image Registration. *IEEE Trans Med Imaging.* 2010;29(1):196–205

28. Kramer CM, Barkhausen J, Bucciarelli-Ducci C, Flamm SC, Kim RJ, Nagel E. Standardized cardiovascular magnetic resonance imaging (CMR) protocols: 2020 update. *J Cardiovasc Magn Reson.* 2020;22:17

29. Liao JR, Pauly JM, Brosnan TJ, Pelc NJ. Reduction of Motion Artifacts in Cine MRI Using Variable-Density Spiral Trajectories. *Magn Reson Med.* 1997;37:569–75

30. Lustig M, Donoho D, Pauly JM. Sparse MRI: the application of compressed sensing for rapid MR imaging. *Magn Reson Med.* 2007;58(6):1182–1195

31. Luijnenburg SE, Robbers-Visser D, Moelker A, Vliegen HW, Mulder BJM, Helbing WA. Intra-observer and interobserver variability of

biventricular function, volumes and mass in patients with congenital heart disease measured by CMR imaging. *Int J Cardiovasc Imaging.* 2010;26:57–64

32. Madelin G, Lee JS, Regatte RR, Jerschow A. Sodium MRI: Methods and applications. *Prog Nucl Magn Reson.* 2014;79:14–47

33. Malayeri AA, Johnson WC, Macedo R, Bathon J, Lima JAC, Bluemke DA. Cardiac Cine MRI: Quantification of the Relationship Between Fast Gradient Echo and Steady-State Free Precession for Determination of Myocardial Mass and Volumes. *J Magn Reson Imaging.* 2008;28:60–66.

34. McRobbie DW, Moore EA, Graves MJ, Prince MR. MRI From Picture to Proton, chapter 8. *Cambridge University Press.* 2006;ISBN 978-0-521-86527-2

35. Myronenko A, Song X. Intensity-Based Image Registration by Minimizing Residual Complexity. *IEEE Trans Med Imaging.* 2010; 29(11):1882–91

36. Nayak KS. Response to letter to the editor: "Nomenclature for real-time magnetic resonance imaging". *Magn Reson Med.* 2019;82:525–526

37. Otazo R, Candès E, Sodickson DK. Low-rank plus sparse matrix decomposition for accelerated dynamic MRI with separation of background and dynamic components. *Magn Reson Med.* 2015;73:1125–36.

38. Plein S, Bloomer TN, Ridgway JP, Jones TR, Bainbridge GJ, Sivanathan MU. Steady-state free precession magnetic resonance imaging of the heart: comparison with segmented k-space gradient-echo imaging. *J Magn Reson Imaging.* 2008;28(1):60–6

39. Portmann J, Wech T, Eirich P, Heidenreich JF, Petri N, Petritsch B, Bley TA, Köstler H. Evaluation of combined late gadolinium-enhancement and functional cardiac magnetic resonance imaging using spiral real-time acquisition. *NMR Biomed.* 2022;e4732

40. Raman SV, Marki M, Patel AR, Bryant J, Allen BD, Plein S, Seiberlich N. 30-minute CMR for common clinical indications: a Society for

Cardiovascular Magnetic Resonance white paper. *J Cardiovasc Magn Reson.* 2022;24:13

41. Robison RK, Li Z, Wang D, Ooi MB, Pipe JG. Correction of B_0 eddy current effects in spiral MRI. *Magn Reson Med.*2019;81:2501–13.

42. Seiberlich N, Breuer FA, Blaimer M, Barkauskas K, Jakob PM, Griswold MA. Non-Cartesian data reconstruction using GRAPPA operator gridding (GROG). *Magn Reson Med.* 2007;58:1257–65.

43. Seiberlich N, Breuer F, Blaimer M, Jakob P, Griswold M. Self-Calibrating GRAPPA Operator Gridding for Radial and Spiral Trajectories *Magn Reson Med.* 2008;59:930–5

44. Solomon I. Relaxation Processes in a System of Two Spins. *Phys. Rev.* 1955;99(2):559–65

45. Steeden JA, Kowalik GT, Tann O, Hughes M, Mortensen KH, Muthurangu V. Real-time assessment of right and left ventricular volumes and function in children using high spatiotemporal resolution spiral bSSFP with compressed sensing. *J Cardiovasc Magn Reson.* 2018;20:79

46. Stich M, Wech T, Slawig A, et al. Gradient waveform pre-emphasis based on the gradient system transfer function. *Magn Reson Med.* 2018;80:1521–32

47. Tran-Gia J, Stäb D, Wech T, Hahn D, Köstler H. Model-Based Acceleration of Parameter Mapping (MAP) for Saturation Prepared Radially Acquired Data. *Magn Reson Med.* 2013;70:1524–34

48. Tsao J, Kozerke S. MRI Temporal Acceleration Techniques. *J Magn Reson Imaging.* 2012;36:543–60

49. Usman M, Atkinson D, Odille F, Kolbitsch C, Vaillant G, Schaeffter T, Batchelor PG, Prieto C. Motion Corrected Compressed Sensing for Free-Breathing Dynamic Cardiac MRI. *Magn Reson Med.* 2013;70:504–16

50. Vogel-Claussen J, Rochitte CE, Wu KC et al. Delayed Enhancement MR Imaging: Utility in Myocardial Assessment. *RadioGraphics.* 2006;26:795—810

51. Wang X, Kohler F, Unterberg-Buchwald C, Lotz J, Frahm J, Uecker M. Model-based myocardial T1 mapping with sparsity constraints using single-shot inversion-recovery radial FLASH cardiovascular magnetic resonance. *J Cardiovasc Magn Reson.* 2019;21:60

52. Wang Y, Che X, Ma S. Nonlinear filtering based on 3D wavelet transform for MRI denoising. *EURASIP J Adv.* 2012;2012:40

53. Wech T, Gutberlet M, Greiser A, Stäb D, Ritter CO, Beer M, Hahn D, Köstler H. High-Resolution Functional Cardiac MR Imaging using Density-Weighted Real-Time Acquisition and a Combination of Compressed Sensing and Parallel Imaging for Image Reconstruction. *Fortschr Röntgenstr.* 2010;182:676–81

54. Wech T, Seiberlich N, Schindele A, Grau V, Diffley L, Gyngell ML, Borzì A, Köstler H, Schneider JE. Development of Real-Time Magnetic Resonance Imaging of Mouse Hearts at 9.4 Tesla—Simulations and First Application. *IEEE Trans Med Imaging.* 2016;35(3):912–20

55. Wech T, Tran-Gia J, Rützel F, Klink T, Bley TA, Köstler H. Single-Shot late Gd enhancement imaging of myocardial infarction with retrospectively adjustable contrast and heart-phase. *Magn Reson Imaging.* 2018;47:48–53

56. Wendland MF, Saeed M, Masui T, Derugin N, Higgins CB. First Pass of an MR Susceptibility Contrast Agent through Normal and Ischemic Heart: Gradient-recalled Echo-Planar Imaging. *JMIU.* 1993;3:755–760

57. Zhou R, Yang Y, Mathew RC, et al. Free-breathing cine imaging with motion-corrected reconstruction at 3T using SPiral Acquisition with Respiratory correction and Cardiac Self-gating (SPARCS). *Magn Reson Med.* 2019;82:706–20

Annex

A Publications

Scientific article

Portmann J, Wech T, Eirich P, Heidenreich JF, Petri N, Petritsch B, Bley TA, Köstler H. Evaluation of combined late gadolinium-enhancement and functional cardiac magnetic resonance imaging using spiral real-time acquisition. *NMR in Biomedicine* 2022;e4732

Conference abstract

Portmann, J, Wech, T, Eirich, P, Köstler, H. MOCO-MAP using a TWIRL trajectory. *ESMRMB 2019, 36th Annual Scientific Meeting, Rotterdam, NL, October 3–October 5: Abstracts, Thursday. Magn Reson Mater Phy* 32, 1–105 (2019)

B Affidavit

I hereby confirm that this doctoral thesis, “Accelerated inversion recovery MRI of the myocardium using spiral acquisition", is the result of my own work. I did not receive any help or support from commercial consultants. All sources and / or materials applied are listed and specified in the thesis.

Furthermore, I confirm that this thesis has not yet been submitted as part of another examination process neither in identical nor in similar form.

.....,	.....	.....
Place,	Date	Signature

Eidesstattliche Erklärung

Hiermit erkläre ich an Eides statt, diese Dissertation, “Beschleunigte Inversion-Recovery MR-Bildgebung des Myokards mit spiralen Auslesezügen", eigenständig, d. h. insbesondere selbständig und ohne Hilfe eines kommerziellen Promotionsberaters, angefertigt und keine anderen als die von mir angegebenen Quellen und Hilfsmittel verwendet zu haben.

Ich erkläre außerdem, dass die Dissertation weder in gleicher noch in ähnlicher Form bereits in einem anderen Prüfungsverfahren vorgelegen hat.

....., den		.....
Ort,	Datum	Unterschrift

C Acknowledgments

I count myself lucky to have had the opportunity to work for the Experimental Radiology in the Department of Diagnostic and Interventional Radiology of the University Hospital of Würzburg and on this doctoral project, which is all due to the kindness of Prof. Dr. Herbert Köstler. His patience and enthusiasm for the matter of research in MR imaging constantly procured encouragement and the scope for new ideas, which creates the environment needed for the formation of scientists.

The framework for this thesis was provided by the thesis committee of Prof. Dr. Michael Laßmann and PD Dr. Dr. Bernhard Petritsch. They were invested and offered a lot of time and advice. PD Dr. Dr. Bernhard Petritsch, in particular, more than once supplied me with insights into the medical side of cardiovascular MRI. I should not forget to thank Dr. Nils Petri, who handled the important search for patients to include in the conducted study. My thanks also goes to the Graduate School of Life Sciences, which takes care of its students in a manner I have never encountered in academia before, and which should be rewarded by long-term support and full appreciation by the University of Würzburg.

Beyond that, I have to emphasize the exceptionally positive and friendly working environment of the work group. Firstly, I should name Prof. Dr. Tobias Wech, who laid the foundation of this work and who introduced me to a comprehensive set of tools and scientific background. I greatly benefited from his experience and intuitive problem-solving skills, as will many co-workers past me. Secondly, Dr. Philipp Eirich, who with the development of the trajectory corrected spiral acquisition and the CRISPI reconstruction, already during his own doctoral project, provided an invaluable source of groundwork for MOCO-MAP and IR-CRISPI. I also had the privilege to work together with nearly anybody of the team at that time, Juliana Bibiano, Susanne Gaul, Dr. Julius Heidenreich, Jonas Kleineisel, Katharina Rath, Dr. Julian Richter, Hannah Scholten, Dr. Anne Slawig, Dr. Andreas Weng. They have been supportive without exception and – making me miss the times at the clinic – always in a pleasant and humorous way.

But in the end we owe our family everything and I am able to count some remarkable beings to it, my mother Gundula, who I respect deeply, my father Thomas, who will always bear the title of “Dr." more naturally than me, although it is not written on his name tag, my sisters Annette and Lucia, who share a bond with me that only siblings can understand. But the core of my family, fortunately, now I may see in my wife Elisabeth, who gives more love than anybody could ever return. Also to this list belong my best man and his wife, Jan and Sophie Trinkwalter, who would adopt me, if

they had to. My last and highest thanks go to my brother and friend Jesus Christ, who saved my life and who is always there, when I need somebody to talk to.